

УДК 539.123

NONACCELERATOR EXPERIMENTS  
ON THE SEARCH FOR RARE PROCESSES  
WITH LOW-BACKGROUND DETECTORS

*A. V. Derbin\**

St. Petersburg Nuclear Physics Institute RAS, Gatchina, Russia

*O. Yu. Smirnov\*\**, *O. A. Zaimidoroга\*\*\**

Joint Institute for Nuclear Research, Dubna

INTRODUCTION	604
LOW-BACKGROUND DETECTORS	606
STUDY OF THE NEUTRINO ELECTROMAGNETIC PROPERTIES	609
SEARCH FOR THE ELECTRON DECAY MODE $e \rightarrow \gamma + \nu$	621
EXPERIMENTAL LIMITS ON THE VIOLATION OF THE PAULI EXCLUSION PRINCIPLE	627
LIMITS ON THE NUCLEON DECAYS INTO INVISIBLE CHANNELS	633
EXPERIMENTAL LIMITS ON THE HEAVY NEUTRINO MIXING IN THE ${}^8\text{B}$ DECAY	639
CONCLUSIONS	642
REFERENCES	643

---

\*E-mail: derbin@mail.pnpi.spb.ru

\*\*E-mail: smirnov@lngs.infn.it

\*\*\*E-mail: zaimidor@sunse.jinr.ru

УДК 539.123

## NONACCELERATOR EXPERIMENTS ON THE SEARCH FOR RARE PROCESSES WITH LOW-BACKGROUND DETECTORS

*A. V. Derbin\**

St. Petersburg Nuclear Physics Institute RAS, Gatchina, Russia

*O. Yu. Smirnov\*\**, *O. A. Zaimidoroга\*\*\**

Joint Institute for Nuclear Research, Dubna

The status of the search for rare processes with low-background detectors is reviewed. The discussed experimental results include searches for the neutrino magnetic moment, neutrino decays and electron instability, the search for the violation of the electric and baryon charge conservation, the search for the violation of the Pauli exclusion principle and for new heavy mass eigenstates of neutrino. The new bounds on the probability of these processes obtained with the prototype of the Borexino detector are presented.

Представлен обзор экспериментов по поиску редких процессов на низкофоновых детекторах. Обсуждаемые экспериментальные результаты включают поиски магнитного момента нейтрино, распада нейтрино, нестабильности электрона, поиски нарушения закона сохранения электрического и барионного зарядов, поиски нарушения принципа Паули, а также новых массовых состояний нейтрино. Представлены новые пределы на вероятности данных процессов, полученные на прототипе детектора «Борексино».

### INTRODUCTION

The Standard Model (SM) of the electroweak interactions [1] successfully describes the major part of the experimental results. Meanwhile, the SM has a number of intrinsic problems, such as the big number of free parameters, the lack of experimental observation of the Higgs particles, the nonclear situation with the cold dark matter origin, and, finally, the discovery of neutrino oscillations. All these facts are challenging experimenters to search for the phenomena outside the SM frames. The search for rare processes in the low-energy region, usually named «nonaccelerating physics», is a method for reaching, maybe in an indirect

---

\*E-mail: derbin@mail.pnpi.spb.ru

\*\*E-mail: smirnov@lngs.infn.it

\*\*\*E-mail: zaimidor@sunse.jinr.ru

way, the energies at which unification of particles and fields occurs, and which are nonreachable for the modern and future particle accelerators. In the present paper we review the results of the searches for the neutrino magnetic moment and neutrino decays, the violation of the electric and baryon charge conservation, the violation of the Pauli exclusion principle (PEP) [2], and the searches for new heavy mass eigenstates of the neutrino.

**Neutrino Magnetic Moment and Solar Antineutrino Flux.** The interest in the huge ( $\sim 10^{-11}\mu$ ) for the SM neutrino magnetic moment was inspired by the solar neutrino problem. The model of spin-flavour precession has had better agreement with experimental data than the oscillation solution, favoured by the KamLAND experiment. At the same time, the oscillation (LMA MSW) solution of the problem does not exclude the possibility of observing weaker effects caused by the neutrino magnetic moment. Anomalously big electromagnetic neutrino moment should lead to the neutrino scattering on the electron and to the radiative neutrino decay  $\nu_H \rightarrow \nu_L + \gamma$ . Another possible manifestation of a large neutrino magnetic moment would be the presence of the antineutrino in the solar neutrino spectrum.

**Electric and Baryon Charge Conservation.** Many extensions of the SM include interactions violating the baryon and lepton charge  $B$  and  $L$ , and are predicting processes with  $\Delta B = 1, 2$  and  $\Delta(B - L) = 0, 2$  resulting in the decay of protons and neutrons in nuclei. The main direction of the searches are the attempts to observe the nucleon decay into strongly interacting charged particles. At the same time, for the processes with nucleon disappearance or decay into weakly interacting particles (neutrinos, majorons, etc.) the experimental limits are by 5–6 orders of magnitude lower. A check on the electric and baryonic charge conservation can be performed by looking for the electron decay into the channel  $e \rightarrow \nu + \gamma$ , and by looking for the decay of nucleons and dinucleons into the «invisible» channel  $N \rightarrow 3\nu$ ,  $NN \rightarrow 2\nu$ .

**Pauli Exclusion Principle.** Experiments on the PEP test are either looking for the anomalous atoms or nuclei in a non-Paulian state, or by searching for the radiation accompanying the non-Paulian transitions. One of the ways of the PEP checking is the search for the emission of  $\gamma$ ,  $p$ ,  $n$  and  $\alpha$  particles, following the transition violating the Pauli principle in nuclei, or the search for the non-Paulian  $\beta^-$  and  $\beta^+$  decays.

**Heavy Neutrino.** Before the discovery of the neutrino oscillations with the mixing parameters  $\Delta m_{12} \approx 6 \cdot 10^{-5}$  eV and  $\Delta m_{23} \approx 3 \cdot 10^{-3}$  eV, the search for the mass eigenstates of  $m_2$  and  $m_3$  in the mass range from a few keV up to some MeV was an actual problem because the upper limits on the masses of  $\nu_\mu$  and  $\nu_\tau$ , obtained in the direct experiments are 170 keV and 18 MeV, respectively. At present, the possibility of the existence of new mass eigenstates is supported by the models with a sterile neutrino. The last one in the common case can have an arbitrary mass and can be mixed with three active neutrinos. The search for

the new mass eigenstates of neutrino can be performed looking for the decay  $\nu_H \rightarrow \nu_L + e^+ + e^-$  of the neutrino with a mass bigger than  $2m_e$ .

## 1. LOW-BACKGROUND DETECTORS

The search for any naturally occurring exotic event must be done in large ultra-pure detectors deep underground, well shielded against the external background. The large size and purity of the detector compensates for the rareness of events, while the location deep underground shields cosmic muon background. The remaining muons passing through the detector must be recognized by a specially designed muon detector. Together with these main features, some other common methods are used for the event type recognition (delayed coincidences for the identification of the radiative chains of U–Th; pulse shape discrimination for the  $\alpha$ - $\beta$  discrimination; direction in the Cherenkov and TPC detectors, etc.).

Nonaccelerator detectors are usually capable of doing more than what is originally proposed, complementing accelerator and astroparticle physics. In this section we give a brief review of the real-time solar neutrino detectors.

**1.1. Kamiokande and Super-Kamiokande.** The Super-Kamiokande detector is the scaled version of the earlier nucleon decay detector Kamiokande [3]. It consists of an inner volume with 18000 t of purified water surrounded by an outer detector formed by 32,000 t of pure water. The whole construction is mounted at the Kamioka mine 1,000 m underground in a cylindrical volume of 41.4 m in height and 39.3 m in diameter. The outer detector is used as a passive shield against the external radiation and as an active muon-veto detector. The inner detector operates 11,200 photomultiplier tubes (PMTs) of 50 cm in diameter mounted at the bottom, top and sides facing inwards. The PMTs collect Cherenkov light emitted by relativistic particles. Information about particle interactions, such as neutrino interactions or proton decay, can be determined by measuring the direction and intensity of Cherenkov light. Compared to Kamiokande, Super-Kamiokande has ten times the volume and twice the density of PMTs. Construction of the detector was completed in 1995 and observation began on April 1, 1996. Energy Resolution of the Super-Kamiokande detector is 16% (at 10 MeV) and its energy threshold is 5 MeV.

The main task of the Super-Kamiokande detector is the proton decay search and solar neutrino observation. The data of Super-Kamiokande have been used to set new limits on the  $^8\text{B}$  neutrino magnetic moment, the antineutrino flux from the Sun, and the  $n - 3\nu$  decays in the Earth, as well as the search for violations of the Pauli Exclusion Principle (PEP) in the  $^{16}\text{O}$  nucleus.

**1.2. KamLAND Detector.** KamLAND [4] is a long baseline reactor anti-neutrino experiment, which discovered neutrino oscillations with the LMA parameters [5]. It is installed at the site of the earlier Kamiokande at a depth of

2700 m of water equivalent. The design of the detector is a scaled version of the Borexino project. The neutrino detector is 1 kt of ultrapure liquid scintillator (80% of dodecane and 20% of pseudocumene (1,2,4-Trimethylbenzene) with 1.52 g/l of PPO (2,5-Diphenyloxazole) as a fluor) contained in a 13 m-diameter spherical vessel, made of thin transparent nylon, concentric with a 18 m-diameter stainless-steel vessel filled with a buffer liquid of dodecane and isoparaffin oil. The buffer protects the LS from the external radiation. The detector is viewed by an array of 1,879 PMT (1,325 specially designed fast 17" PMTs and 554 older 20" Kamiokande PMTs). The total geometrical coverage is 34%, but in the first analysis [5] only the large area PMTs (17") were used, which corresponded to 22% of the geometrical coverage. The observed energy resolution is  $7.5\%/\sqrt{E(\text{MeV})}$ , and the analysis threshold is set at 2.6 MeV.

There are plans to purify the LS of the KamLAND to the levels permitting the search for the solar  ${}^7\text{Be}$ -neutrinos signal [6].

The KamLAND detector is sensitive to the terrestrial antineutrino, galactic supernova neutrino, nucleon and dinucleon decays into the invisible channels, its data have been used to set the best to date limit on the solar antineutrino flux.

**1.3. SNO Detector.** The Sudbury Neutrino Observatory (SNO) detector [7] was built 2040 m (6000 m water equivalent) under ground, in INCO's Creighton mine near Sudbury, Ontario. The SNO is a heavy-water Cherenkov detector, sensitive to the neutrino neutral currents. It uses 1000 t of heavy water, contained in a 12 m-diameter acrylic vessel. The Cherenkov light is detected by an array of 9600 photomultiplier tubes mounted on a support structure. The detector is immersed in 7400 t of ultrapure light water within a 30 m barrel-shaped cavity. Special measures were undertaken in order to ensure the absence of radioactive background from the elements present in the mine dust.

Together with the observation of neutral and charged currents from the solar neutrino, the best limits on the proton decay into the invisible channel have been established with the SNO data.

**1.4. Borexino Counting Test Facility (CTF).** The CTF is a prototype of the Borexino detector. Borexino, a real-time 300 t detector for low-energy neutrino spectroscopy, is nearing completion in the Gran Sasso Underground Laboratory (see [8] and refs. therein). The main goal of the detector is the measurement of the  ${}^7\text{Be}$  solar neutrino flux via  $\nu - e$  scattering in an ultra-pure liquid scintillator, while several other basic questions in astro- and particle physics will also be addressed. Detailed reports on the CTF results have been published [8–10].

The Borexino collaboration has operated 3 versions of the CTF detector. The first one took data in 1994–1995 and addressed mainly the technical problem of deep purification of large volumes of water and scintillator. The upgraded version of the CTF (CTF-II) was equipped with a muon veto detector, its data acquired in 2000 were used in the search for electron decay  $e \rightarrow \nu + \gamma$ , non-Paulian transitions for the nuclei, nucleon and dinucleon decays into invisible channels,

electromagnetic properties of neutrino, and neutrino decays. At present, the third modification of the detector continues to take data.

The CTF consists of an external cylindrical water tank ( $\varnothing 11 \times 10$  m;  $\approx 1000$  t of water) serving as a passive shielding for a  $4.2 \text{ m}^3$  liquid scintillator (LS) contained in an inner spherical vessel of  $\varnothing 2.0$  m. High purity water with a radio-purity of  $\approx 10^{-14}$  g/g in U/Th,  $\approx 10^{-12}$  g/g in K, and  $< 2 \mu\text{Bq/l}$  for  $^{222}\text{Rn}$  is used for the shielding. The LS was purified to the level of  $\approx 10^{-16}$  g/g in U/Th contamination.

The energy of an event in the CTF detector is defined using the total collected charge from all PMTs. In a simple approach the energy is supposed to be linear with respect to the total collected charge. The coefficient linking the event energy and the total collected charge is called light yield (or photoelectron yield). The light yield for electrons can be considered linear with respect to its energy only for energies above 1 MeV. At low energies the phenomenon of «ionization quenching» violates the linear dependence of the light yield versus energy [11]. The deviations from the linear law can be taken into account by the ionization deficit function ( $f(k_B, E)$ ), where  $k_B$  is Birks' empirical constant. The «ionization quenching» effect leads to a shift in the position of the full energy peak for gammas on the energy scale calibrated using electrons. In fact, the position of the 1461 keV  $^{40}\text{K}$  gamma in the CTF-II data corresponds to 1360 keV of the energy deposited for an electron.

The detector energy and spatial resolution have been studied with radioactive sources placed at different positions inside the active volume of the CTF. A typical spatial  $1\sigma$  resolution is 10 cm at 1 MeV. The studies have showed also that the total charge response of the CTF detector can be approximated by a Gaussian. For energies  $E \geq 1$  MeV the relative resolution can be expressed as  $\sigma_E/E = \sqrt{3.8 \cdot 10^{-3}/E + 2.3 \cdot 10^{-3}}$  ( $E$  is in MeV) [12] for events uniformly distributed over the detector's volume.

The low-energy part of the CTF spectrum is dominated by the  $^{14}\text{C}$  and can be described (in the region up to 350–400 keV) with a high precision by the model consisting of the sum of the  $^{14}\text{C}$  spectrum  $S^\beta$  and the polynomial term:

$$S^{\text{Model}}(Q) = N_0 S^\beta(Q, \{A, k_B, \alpha\}) + a + bQ, \quad (1)$$

with 6 parameters:

- $N_0$  is the number of  $^{14}\text{C}$  decays;
- $A$  is the scintillator light yield measured in p.e./MeV;
- $k_B$  is the quenching factor;
- $\alpha$  is the  $^{14}\text{C}$  shape factor ( $\text{MeV}^{-1}$ );
- $a, b$  are the parameters describing the linear background underlying the residual spectrum.

The endpoint energy of the  $^{14}\text{C}$  spectrum was fixed at the value measured in other experiments with sufficient accuracy  $E_0 = (156 \pm 0.5)$  keV.

**1.5.  $2\beta$  Decay and Dark Matter Detectors.** These detectors have essentially smaller (up to 100 kg) mass in comparison with the solar neutrino detectors. For example DAMA collaboration [13] operates two low-background detectors. One of them consists of nine 9.70-kg crystals of low radioactive NaI(Tl). Four 7.05-kg older detectors placed at the top, are mainly used as special triggers. All the materials used in the detectors were accurately selected using the Germanium facility at Gran Sasso, mass and atomic absorption spectrometers, and in situ. The latter method provides the highest sensitivity. Another set-up of the DAMA collaboration is a liquid Xenon scintillator of 6.5 kg filled with Kr-free Xenon enriched in  $^{129}\text{Xe}$  at 99.5%.

With these detectors some new limits have been established, including charge nonconserving processes ( $e \rightarrow \nu + \gamma$ ,  $e \rightarrow 3\nu$ ), nucleon and dinucleon decays into invisible channels and PEP violation processes.

## 2. STUDY OF THE NEUTRINO ELECTROMAGNETIC PROPERTIES

**2.1. Introduction.** The Lorentz-covariant total electromagnetic current for fermions can be presented in the following form [14]:

$$J_\alpha(q) = F(q^2)\gamma_\alpha + G(q^2)(q^2\gamma_\alpha - 2i(q_\alpha))\gamma_5 + M(q^2)\sigma_{\alpha,\beta}q_\beta + iE(q^2)\sigma_{\alpha,\beta}q_\beta\gamma_5, \quad (2)$$

where  $q$  is the energy-momentum transfer to the fermion and the functions ( $q^2$ ),  $G(q^2)$ ,  $M(q^2)$ , and  $E(q^2)$  represent the electromagnetic, anapole, magnetic and electric dipole form factors, respectively. In the limit  $q \rightarrow 0$ ,  $F$  is the fermion electric charge,  $M$  is the dipole magnetic moment and  $E$  is the electric dipole moment of the fermion. In the following we discuss the existing limits on the above electromagnetic form factors for neutrinos.

Assuming electric charge conservation in the neutron decay  $n \rightarrow p + e^- + \bar{\nu}_e$ , experimental measurements of the ( $p + e^-$ ) [15] and  $n$  [16] charge lead to the upper limit  $|e_{\bar{\nu}_e}| \leq 10^{-21}e$ . From astrophysical considerations, including solar and SN1987A data, the limits on the neutrino charge are less stringent  $e_\nu \leq 10^{-13} \div 10^{-17}e$  [17, 18].

The charge radius of the neutrino  $\langle r^2 \rangle \simeq 6 \frac{\delta F(q^2)}{\delta q^2} \Big|_{q^2=0}$  (as well as the anapole moment for the Majorana neutrino) is induced by radiative corrections in the Standard Model of electroweak interactions (SM) and has a value equal to  $\frac{G_F}{2\sqrt{2}\pi^2} \ln \frac{M_W^2}{m_e^2} \sim 3.2 \cdot 10^{-33} \text{ cm}^2$  for the electron neutrino [19, 20]. Modern accelerator experiments studying the  $\nu_\mu - e$  scattering have sensitivity a few

times poorer than needed to see the effect of these radiative corrections. The charge radius of the electron and muon neutrino has a bound of  $-2.97 \cdot 10^{-32} \leq \langle r^2 \rangle \leq 4.14 \cdot 10^{-32} \text{ cm}^2$  [21,22] and  $|\langle r^2 \rangle| \leq 6 \cdot 10^{-33} \text{ cm}^2$  [23,24], respectively. From Super-Kamiokande and SNO data the charge radius is limited at values  $\leq 6.9 \cdot 10^{-32} \text{ cm}^2$  [25]. Moreover, from the same data, taking into account that  $\mu_\nu$  and  $\langle r^2 \rangle$  are correlated, it is found:  $-1.2 \cdot 10^{-32} \leq \langle r^2 \rangle \leq 2.7 \cdot 10^{-32} \text{ cm}^2$ , when  $\mu_\nu = 0$  for Dirac neutrinos [26].

A nonzero neutrino electric dipole moment,  $d_\nu = E(0)$ , is *CP* violating and, up to now, such a moment has not been observed for any particle. Both dipole moments,  $(\mu_\nu, d_\nu)$ , are forbidden for Majorana neutrinos in the case of *CPT*-invariance.

The neutrino magnetic moment  $\mu_\nu = M(0)$  in the SM is proportional to the neutrino mass. The value of  $\mu_\nu$  is

$$\mu_\nu = \frac{3m_e G_F}{4\pi^2 \sqrt{2}} m_\nu \mu_B \approx 3.2 \cdot 10^{-19} \left( \frac{m_\nu}{1 \text{ eV}} \right) \mu_B, \quad (3)$$

where  $\mu_B$  is the electron Bohr magneton. The current limit on the neutrino mass is 2.2 eV [27,28], hence the neutrino magnetic moment calculated in the SM is less than  $10^{-18} \mu_B$ .

The elastic scattering of a neutrino by an electron turns out to be the most sensitive reaction to search for a nonzero neutrino magnetic moment. The measured cross sections for this process set the restriction  $\mu_{\bar{\nu}_e} \leq 1.0\text{--}4.0 \cdot 10^{-10} \mu_B$  on a possible magnetic moment for electron antineutrinos [29–37],  $\mu_{\nu_e} \leq 1.1 \cdot 10^{-9} \mu_B$  for electron neutrinos [21,38],  $\mu_{\nu_\mu} \leq 6.8 \cdot 10^{-10} \mu_B$  for muon neutrinos [38,39], and  $\mu_{\nu_\tau} \leq 3.9 \cdot 10^{-7} \mu_B$  for tau neutrinos [40].

As far as solar neutrinos are concerned, an upper bound for a magnetic moment using  $^8\text{B}$  neutrinos was obtained in [41],  $\mu_\nu \leq 2.2\text{--}2.3 \cdot 10^{-10} \mu_B$  using data from Super-Kamiokande, Kamiokande and Homestake. A more recent analysis of the Super-Kamiokande  $^8\text{B}$  data sets an upper limit on the neutrino magnetic moment at the level of  $(1.0\text{--}3.6) \cdot 10^{-10} \mu_B$  (90% CL) [42,43].

The resonant spin-flavour precession (RSFP) of solar neutrinos due to the interaction of their transition magnetic moments with the solar magnetic field provided, was a suitable solution to the solar neutrino problem with  $\mu_\nu \simeq 10^{-11} \mu_B$  [44–46].

The most stringent limits on the neutrino magnetic moment in the range of  $10^{-12} \text{--} 10^{-10} \mu_B$  come from astrophysical observations ([17,18] and references therein).

## 2.2. The Problem of the Solar Neutrino and Neutrino Magnetic Moment.

At present, the data of 6 solar neutrino experiments are available. Three of them are radiochemical experiments, a Cl–Ar and two Ga–Ge ones, detecting neutrinos from the inverse *e* capture. Two detectors are registering Cherenkov light produced by the recoil electrons (Kamiokande and Super-Kamiokande). The SNO

detector is also sensitive to the reactions with neutral currents, it is registering neutrinos by the deuteron fragmentation ( $\nu d, np$ ) and by the ( $\nu, e$ ) scattering. The solar neutrino fluxes measured in all the experiments are presented in Table 1 as a ratio (or in comparison with) the predictions of the SSM [47]. The first error cited in the Table has a statistical origin, and the other one is due to the uncertainties in the theoretical calculations.

**Table 1. Results of solar neutrino flux measurements in comparison with the predictions of the SSM**

Cl–Ar, Homestake [48]	$0.28 \pm 0.02 \pm 0.04$
Ga–Ge, SAGE [49]	$(70.8 \pm 5.3 \pm 3.7)/128$
Ga–Ge, GALLEX/GNO [50]	$(70.8 \pm 4.5 \pm 3.8)/128$
Kamiokande [51]	$0.42 \pm 0.06 \pm 0.07$
Super-Kamiokande [52]	$0.37 \pm 0.02 \pm 0.07$
SNO [53]	CC: $0.35 \pm 0.002$ , NC: $1.01 \pm 0.13$

One of the proposed explanations of the solar neutrino deficit has been the assumption of the big neutrino magnetic moment. In this case the interaction with the solar magnetic field would lead to the helicity flip, and, as a result, to reduction in the observed flux of solar neutrinos due to the sterility of the right neutrino with respect to the charged current reactions [54, 55]. 10 years after the start of the Cl–Ar experiment, this idea was strongly supported by the observation [56, 57] of a possible anticorrelation of the registered neutrino flux and the number of solar spots. The solar spots are the visible result of the solar magnetic field activity, the number of the spots is connected with the magnetic field tension near the surface of the Sun.

In 1986 Voloshin, Vysotsky, and Okun [59–61] put forward an assumption that this anticorrelation can be explained by the interaction of the neutrino magnetic moment with the solar magnetic field in the convective zone. The convective zone occupies approximately a quarter of the radius of the Sun close to the surface. The active Sun generates the toroidal magnetic field with a strength  $H$  of 1–10 kGs. The neutrino spin is precessing in the magnetic field oriented perpendicular to the direction of movement, and the left-handed neutrinos are converted to the right-handed ones. The number of the left-handed neutrinos leaving the Sun can be estimated using a simple formula  $N \sim \cos^2(\mu_\nu H L)$ , where  $L$  is the depth of the convective zone ( $L \approx 2 \cdot 10^{10}$  cm). Thus, the magnetic moment value necessary for the observation of the 11-year and 6-month periodic variations of the solar neutrino fluxes with the modern solar neutrino detectors lies in the range  $10^{-10}$ – $10^{-12} \mu_B$ . The value of  $10^{-10} \mu_B$  is eight orders of magnitude higher

than the value predicted by the SM, but does not contradict the limit obtained in laboratory experiments.

In [62] it was demonstrated that anticorrelation of the neutrino flux is more significant for the absolute value of the magnetic flux at the surface of the Sun than for the number of solar spots. Moreover, it is more significant for the magnetic flux in the vicinity of the center of Sun's visible disk. The Cl–Ar experiment registered mainly neutrinos appearing in the  $\beta^+$  decay of  $^8\text{B}$  and in  $K$  capture on  $^7\text{Be}$ . These reactions occur in the core of the Sun, in the region which is 5 times smaller than the region of the  $pp$  reactions. Hence, the  $^8\text{B}$  and  $^7\text{Be}$  neutrinos pass the surface of the Sun near the centre of the visible disk on their way to the Earth. Because of the big uncertainties in the Cl–Ar experiment data, the quantitative evaluation of the correlation coefficient is a very complicated task. The standard correlation coefficient, calculated in [56] and [57], corresponds to the  $\sim 99\%$  CL.

Other solar neutrino detectors — Sage, Gallex, and Kamiokande — did not observe significant 11-years or 6-month correlations between the registered neutrino flux and magnetic activity of the Sun. If the correlation really takes place, then the reason for this discrepancy could be the different energy ranges registered by all these detectors. The threshold of the Cl–Ar experiment is 814 keV, the threshold of the Ga–Ge detector is 233 keV and the threshold of the Kamiokande detector is 6.5–7 MeV. The analysis of the data taken in the Cl–Ar, Ga–Ge and Super-Kamiokande experiments was continued in [63,64]. The time variations of the neutrino flux registered by these detectors, due to the rotation of the Sun with a period of  $\simeq 28$  days, were considered in [65].

As noted above, in the case of mixing the neutrino along the diagonal magnetic moment should have nondiagonal (transition) magnetic moments. The nondiagonal magnetic moment is possible both for the Majorana neutrino and for the Dirac neutrino. Akhmedov, Lim, and Marciano [44,45] demonstrated that the spin-flavour precession of the neutrino in the magnetic field of the Sun can have a resonant character similar to the MSW effect. Taking into account the resonance oscillations in matter, the probability of the  $\nu_L \rightarrow \nu_R$  transition will depend on the neutrino energy and comparison of experimental data taken with different detectors complicates significantly. The analysis of the data of all the solar neutrino detectors for the case of spin-flavour precession performed in [46,66–68] resulted in the  $\chi^2$  value which is lower than that for the LMA MSW solution. At the same time, the oscillation solution of the problem does not exclude the possibility of observing subdominant effects caused by the neutrino magnetic moment.

**2.3. Constraints on the Solar Antineutrino Flux and Neutrino Magnetic Moment.** A possible manifestation of a large neutrino magnetic moment would be the presence of the antineutrino in the solar neutrino spectrum. The mechanism of the neutrino–antineutrino conversion due to the spin-flavour precession (SFP) induced by the neutrino transition magnetic moment was discussed in [44,45,69].

An alternative model of antineutrino production in  $\nu$  decays in models with spontaneous violation of the lepton number was considered in [70–73].

The inverse beta-decay of the antineutrino  $\bar{\nu}_e + p \rightarrow n + e^+$  is the dominant type of antineutrino interactions in a large volume Cherenkov or liquid scintillator detectors. The cross section for this process is two orders of magnitude higher than that for the antineutrino elastic scattering. The capture of the thermalized neutron on the proton  $n + p \rightarrow d + \gamma$  with a mean capture-time of  $\sim 170 \mu\text{s}$  and the energy release  $E_\gamma = 2.2 \text{ MeV}$  provides a tag for this reaction in an LS detector, allowing operation at a practically zero background. In a water Cherenkov detector the delayed 2.2 MeV gamma is below the threshold, and a positron from the inverse beta decay is indistinguishable from an electron or gamma. In this case solar neutrinos and spallation products contribute to the background, and the sensitivity of the detector is much worse in comparison even with a smaller volume LS detector. In fact, the recent Super-Kamiokande (water Cherenkov detector) limit for the solar antineutrino flux  $\phi_{\bar{\nu}_e} < 0.8 \cdot 10^{-2}$  in the energy region  $8 < E_\nu < 20 \text{ MeV}$  at 90% CL [74] was dramatically improved by a factor of 30 by the KamLAND (LS detector) collaboration. The most stringent constraints on the solar antineutrino flux  $\phi_{\bar{\nu}_e}$  from the KamLAND data are  $\phi_{\bar{\nu}_e} < 2.8 \cdot 10^{-4}$  at 90% CL in the energy region  $8.3 < E_{\bar{\nu}_e} < 14.8 \text{ MeV}$ . The expected background for the KamLAND detector was as small as  $1.1 \pm 0.4 \text{ eV}/(0.28 \text{ kt} \cdot \text{y})$  and no candidate events were observed; in the Super-Kamiokande detector the rate of candidate events was 29781 during 1496 days of data taking in a 22.5 kt fiducial volume with a background of  $(2.77 \pm 0.20) \cdot 10^4$  due to spallation events.

The constraints on the neutrino transition magnetic moment can be obtained from this limit assuming that the MSW scenario is dominant in the formation of the solar neutrino flux with the parameters corresponding to the LMA in the parameter space, and that the SFT mechanism is responsible for the antineutrino flux. If the transverse component of the solar magnetic field is  $B_T$  at a radius of  $0.05R_\odot$ , then [75]

$$\mu_\nu < 1.3 \cdot 10^{-9} \frac{10 \text{ kGs}}{B_T(0.05R_\odot)}.$$

In the case of random magnetic fields inside the Sun, the upper bound on  $\mu_\nu$  lies in the region of  $\mu_\nu < 1.5 - 5 \cdot 10^{-12} \mu_B$  [76].

**2.4. Neutrino–Electron Elastic Scattering.** Neutrino–electron elastic scattering is the most sensitive test for a neutrino magnetic moment search. In the SM, the scattering of a neutrino with a nonzero magnetic moment is determined both by the weak interaction term and by the one-photon exchange contribution. The latter changes the helicity of the final neutrino state. Therefore, the amplitudes of the weak and electromagnetic scattering do not interfere, at least at the level of  $\sim m_\nu/E_\nu$ , and the total cross section is the sum of two cross sections.

The differential cross section for the weak contribution to neutrino–electron elastic scattering has the form:

$$\frac{d\sigma_W}{dT_e}(T_e, E_\nu) = 4\sigma_0 \left[ g_L^2 + g_R^2 \left( 1 - \frac{T_e}{E_\nu} \right)^2 - g_L g_R \frac{T_e m_e}{2E_\nu^2} \right], \quad (4)$$

where  $\sigma_0 = \frac{G_F^2 m_e}{2\pi} = 4.28 \cdot 10^{-45} \text{ cm}^2/\text{MeV}$ ; the values of  $g_R$  and  $g_L$  depend only on the Weinberg angle ( $\sin^2 \theta_W = 0.2315$ ) with  $g_L = g_V + g_A = 1/2 + \sin^2 \theta_W$ ,  $g_R = g_V - g_A = \sin^2 \theta_W$ ; and  $E_\nu$  and  $T_e$  are the energies of the incident neutrino and the recoil electron. The scattering due to the charge radius interferes with the weak scattering contribution. In this case the parameters  $g_R$  and  $g_L$  are modified in accordance with the new values of  $g'_V = g_V + x$ , where  $x = \frac{\sqrt{2}\pi\alpha}{3G_F} \langle r^2 \rangle = 2.38 \cdot 10^{30} \langle r^2 \rangle \text{ cm}^2$ .

The  $\nu$ – $e$  scattering cross section associated with the magnetic moment is:

$$\frac{d\sigma_{\mu_\nu}}{dT_e}(T_e, E_\nu) = \pi r_0^2 \mu_\nu^2 \left( \frac{1}{T_e} - \frac{1}{E_\nu} \right), \quad (5)$$

where  $\mu_\nu$  is the neutrino magnetic moment measured in  $\mu_B$  units, and  $r_0 = 2.818 \cdot 10^{-13} \text{ cm}$  is the classical electron radius.

In the case of mixing, the effective magnetic moment of the neutrino is given by the following formula [42–45, 77]:

$$\mu_{\text{eff}}^2 = \sum_j \left| \sum_k \mu_{jk} A_j(E_\nu, L) \right|^2, \quad (6)$$

where  $\mu_{jk}$  is the fundamental matrix which characterizes the neutrino electromagnetic coupling;  $A_k(E, L)$  is the probability amplitude of the neutrino mass eigenstate  $\nu_k$  at the detector. In the general case  $A_k(E, L)$  (and  $\mu_{jk}^2$ ) might depend not only on the mixing angles but also on the neutrino energy and source-detector distance  $L$ .

For the vacuum oscillations  $A_k(E, L) = U_{ek} e^{-iE_k L}$ , where  $U_{ek}$  is an element of the mixing matrix. The flavor eigenstates  $\nu_l$  ( $l = e, \mu, \tau$ ) are related to the mass eigenstates  $\nu_i$  by virtue of the unitary mixing matrix  $U$ :  $\nu_l = \sum_{i=1}^3 U_{li} \nu_i$ .

With reasonable assumptions in the case of vacuum oscillations  $\mu_{jk}^2$  has no dependence on  $L$  and  $E_\nu$  and depends only on  $\mu_{jk}$  and the vacuum mixing  $U_{ek}$ .

In particular, for Dirac neutrinos  $\mu_\nu^2 = \sum_{k=1}^3 |U_{ek}|^2 |\mu_{kk}|^2$ . For Majorana neutrinos  $\mu_\nu^2 = |\mu_{12}|^2$  [42], taking into account only two relevant mass eigenstates.

If oscillations of the solar neutrino are caused by the MSW mechanism, then  $A_k(E, L)$  is defined by the mixing angle in the matter of the Sun  $\theta_m$ :

$$\tan 2\theta_m = \frac{\sin 2\theta}{\cos 2\theta + (L/L_e)}, \quad (7)$$

where  $L$  is the length of oscillations in vacuum,  $L = 4\pi E_\nu / \Delta m_{12}^2$ ;  $L_e$  is the length of neutrino–electron interaction,  $L_e = 2\pi / (\sqrt{2} G_f N_e)$ . Thus,  $A_k(E, L)$  depends only on  $E_\nu$  and  $\Delta m_{12}^2$ . For three light neutrinos, the effective magnetic moment is [42–45, 77]:

$$\mu_\nu^2 = P_{e1} \mu_{11}^2 + (1 - P_{e1}) \mu_{22}^2 + \mu_{12}^2 + P_{e1} \mu_{13}^2 + (1 - P_{e1}) \mu_{23}^2, \quad (8)$$

where  $P_{e1} = |A_1(E, L)|^2$  is the probability of the  $\nu_e \rightarrow \nu_1$  transition after crossing the resonant region.

All the elements of the matrix  $\mu_{jk}$ , with exception of  $\mu_{33}$ , can be limited using the bounds on the  $\mu_\nu^2$  and  $P_{e1}$  value, and noting that formula (8) contains only positive terms. For the LMA solution the value of  $P_{e1}$  for the  ${}^7\text{Be}$  neutrino is close to 0.5. As follows from equation (8), the value  $P_{e1} = 0.5$  leads to more stringent limits on the sum of the squares of the transition moments  $\mu_{12}^2 + \mu_{23}^2 + \mu_{13}^2$  in the case of the Majorana neutrino and to more stringent limits on the sum of the squares of the diagonal moments  $\mu_{11}^2 + \mu_{22}^2$  for the Dirac neutrino. In this way, detectors capable to register low energy solar neutrinos are more sensitive to the neutrino magnetic moment.

The energy dependence of the cross sections for the magnetic and weak scattering differs significantly; for  $T_e \ll E_\nu$  their ratio is proportional to  $1/T_e$ , i.e., a decrease of the electron detection threshold will increase the sensitivity of the experiment to the magnetic moment.

### 2.5. Upper Limit on the Magnetic Moment of $pp$ and ${}^7\text{Be}$ Neutrinos.

The upper limit on the magnetic moment of low energy solar neutrinos was obtained with the Counting Test Facility (CTF) [78]. To get the expected energy spectrum of the recoil electrons in the detector it is necessary to fold cross sections (4) and (5) with the neutrino spectrum and detector response function. In the calculations the neutrino fluxes given by the Standard Solar Model (SSM) [79] and neutrino energy spectra from [80] were used. The detector response function was studied in [12].

The expected spectra for the SSM neutrino weak contribution,  $S^W(Q)$ , and the magnetic one,  $S^{\mu\nu}(Q)$  (for  $\mu_\nu = 10^{-9} \mu_B$ ), are shown in Fig. 1. The spectra are calculated using the cross sections (4) and (5) folded with corresponding solar neutrino spectra and taking into account the detector's response function. The total number of target electrons in the CTF-II is  $N_e = 1.36 \cdot 10^{30}$ , the time of data taking  $T = 32.1$  days; the total efficiency of the detector  $\varepsilon = 0.67$  is defined by the spatial cut applied and the dead time of the electronics.

If the total rate in the energy region around 220 keV (Fig. 1) is attributed to the neutrino magnetic scattering, then a conservative estimate of the neutrino magnetic moment is  $\mu_\nu = 1.2 \cdot 10^{-9} \mu_B$ . Different energy dependence of the background spectrum and the spectrum of the recoil electrons due to the magnetic scattering was used in the analysis. An energy interval of 185–380 keV was chosen for analysis to select the region with the maximal statistical significance of the expected effect while minimizing the additional systematic uncertainties related to the linear background which increases at lower energies.

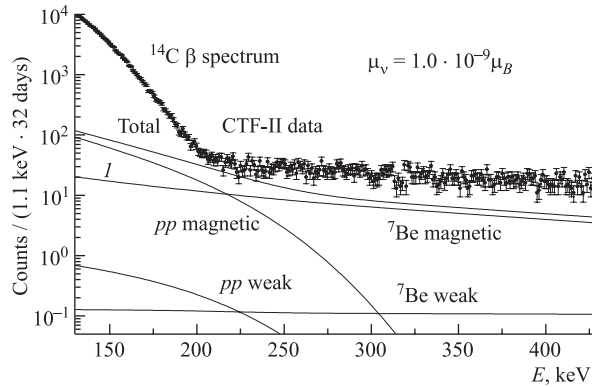


Fig. 1. The experimental spectrum measured by the CTF-II (the upper plot with error bars) and the expected spectra for the magnetic and weak scattering of  $pp$  and  ${}^7\text{Be}$  neutrinos calculated in accordance with (4), (5)

An analysis of the upper limit for a possible magnetic moment of the neutrino was performed by minimizing  $\chi^2$  for different values of  $\mu_\nu^2$ . The minimum of  $\chi^2$  corresponds to  $\mu_\nu = 3.2 \cdot 10^{-10} \mu_B$ ;  $\mu_\nu \leq 0$  has a probability of 40%. The probability function was renormalized to the physical region  $\mu_\nu^2 \geq 0$ , in accordance with the recommendations of the Particle Data Group [18]. The integration of the probability function gives 0.9 (90% CL) for  $\mu_\nu = 5.5 \cdot 10^{-10} \mu_B$ . So the limit is practically independent of the lower bound of the analyzed region. The fit with an exponential underlying background gives a slightly stronger limit on the  $\mu_\nu = 5.0 \cdot 10^{-10} \mu_B$ . So the limit is practically independent of the model chosen. The results of the best fit for  $\mu_\nu = 5.5 \cdot 10^{-10} \mu_B$  are shown in Fig. 2. The neutrino magnetic moment of  $\mu_\nu = 5.5 \cdot 10^{-10} \mu_B$  (excluded at 90% CL) would yield about 20% of the total background in the region of 200–250 keV. This low «signal-to-noise» sensitivity is explained by the similarity of the shapes of the background and the magnetic moment effect (a linear function with a small negative slope), and by the impossibility to perform «background only» measurements with the Sun «switched off», as in the reactor experiments.

This limit is only about 3 times worse compared to the 825-day Super-Kamiokande result [42], and is the first one obtained with sub-MeV neutrinos in a direct experiment. As one can see from Fig. 1 (line *I*), the limit on the magnetic moment with the Borexino detector will be improved by one order of magnitude if Borexino achieves sensitivity to  ${}^7\text{Be}$  neutrinos.

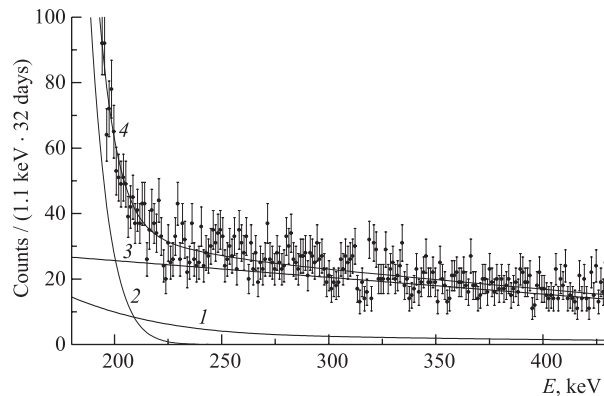


Fig. 2. Fit in the region of 185–380 keV for  $\mu_\nu = 5.5 \cdot 10^{-10} \mu_B$ . *I* — spectrum of recoil electrons due to magnetic scattering; 2 —  ${}^{14}\text{C}$   $\beta$  spectrum; 3 — linear background; 4 — total fit

The sensitivity of the CTF detector to the potential neutrino charge radius was tested in [78]. In accordance with (4) the energy spectrum of recoil electrons has the same shape as in the case of the weak scattering. For this reason, the low energy threshold of the CTF-II offers no advantage in searching for the neutrino charge radius. The upper limit obtained is  $\langle r^2 \rangle \leq 2.2 \cdot 10^{-30} \text{ cm}^2$  (90% CL). The expected spectrum of the recoil electrons for this value of the charge radius is shown in Fig. 4. The result is poorer than the one obtained in accelerator experiments [21–24] and with  ${}^8\text{B}$  solar neutrinos [25, 26].

**2.6. Search for the Neutrino Radiative Decay  $\nu_H \rightarrow \nu_L + \gamma$ .** If neutrinos have mass, then the heavier one can decay to a lighter one. At a mass of the heavy neutrino  $m_{\nu_H} \geq 2m_e$  the dominant mode is the decay into an electron, a positron and a light neutrino  $\nu_H \rightarrow e^+ + e^- + \nu_L$ . For a neutrino with a mass below  $2m_e$ , the radiative decay  $\nu_H \rightarrow \nu_L + \gamma$  is the only viable process for direct detection. The Feynman graphs describing the radiative decay are the same that contribute to the neutrino magnetic moment. In the Standard Model (SM), the lifetime of the radiative neutrino decay expressed in terms of the transition

magnetic moment  $\mu_{HL}^r$  is [81–84]:

$$\tau[\text{s}] \approx 0.19 \left( \frac{\mu_B}{\mu_{HL}^r} \right)^2 \left( \frac{m_{\nu_H}^2}{m_{\nu_H}^2 - m_{\nu_L}^2} \right)^3 \left( \frac{1 \text{ eV}}{m_{\nu_H}} \right)^3, \quad (9)$$

where  $\mu_{HL}^r$  is expressed in Bohr magneton ( $\mu_B$ ) units. The probability of radiative decay in the SM is very low. If the neutrino transition moment  $\mu_{HL}^r$  has a value close to that expected for the diagonal magnetic moment  $\mu_\nu \approx 3.2 \cdot 10^{-19} \left( \frac{m_\nu}{1 \text{ eV}} \right) \mu_B$ , then from (9) the lifetime of the neutrino is  $\tau \sim 10^{29}$  y. At the same time, the reasons (the same as for right-handed weak interactions) leading to a large magnetic moment also lead to an increase in the probability of the radiative neutrino decay [85–88].

The radiative decay of the reactor antineutrinos  $\bar{\nu}_e$  was studied in [34, 89–92]; the latter gives the strongest lifetime lower limit of  $\tau_{\text{cm}}/m_\nu \geq 200 \text{ s} \cdot \text{eV}^{-1}$  (90% CL). The search for the  $\nu\mu$  and  $\bar{\nu}_\mu$  decays was performed in a high intensity beam of neutrinos produced by  $\pi^+$  and  $\mu^+$  decay at rest; the lifetime of the muon (anti)neutrino was bounded at the value  $\tau_{\text{cm}}/m_{\nu_\mu} \geq 15.4 \text{ s} \cdot \text{eV}^{-1}$  [93]. A much more restrictive limit was obtained from the solar  $\gamma$ -ray flux,  $\tau_{\text{cm}}/m_{\nu_e} \geq 7 \cdot 10^9 \text{ s} \cdot \text{eV}^{-1}$  [94]. The astrophysical limits are even stronger, and lie in the region of  $10^9$ – $10^{20} \text{ s} \cdot \text{eV}^{-1}$  ([17, 18] and references therein).

The most stringent direct limits on the neutrino radiative decay were obtained with the Borexino CTF [95, 96]. The analysis was performed on the assumption that the decaying neutrino  $\nu_H$  is dominantly coupled to the electron ( $U_{eH} \approx 1$ ) and in the final state  $\nu_L$  the neutrino mass vanishes (i.e.,  $m_{\nu_L} \ll m_{\nu_H}$ ). The expected laboratory gamma spectrum was defined by the photon moment distribution in the centre-of-mass system. For the common case one can write the photon angular distribution in the general form [90]:

$$dN = \frac{1}{2}(1 + \alpha \cos(\theta)) d \cos(\theta). \quad (10)$$

The anisotropy parameter  $\alpha$  defines the angular distribution of the photon relative to the spin of the decaying neutrino in the neutrino rest frame, and is related to the space-time structure of the decay vertex. For the Majorana neutrino,  $\alpha$  is identically zero ( $\alpha = 0$ ), but can take on any value in the interval  $-1 \leq \alpha \leq 1$  for the Dirac neutrino. With the assumption of total parity violation, the generated left (right)-handed Dirac neutrinos correspond to the case  $\alpha = -1(+1)$ . The lab-frame energy of the decay gamma  $E_\gamma$  in terms of the lab-frame energy of the neutrino  $E_\nu$  and the center-of-mass angle  $\theta$  is:

$$E_\gamma = \frac{E_\nu}{2} \left( 1 + \frac{P_\nu}{E_\nu} \cos(\theta) \right). \quad (11)$$

After the relativistic time dilation one obtains the gamma energy spectrum  $E_\gamma$  due to the decay of a neutrino with the energy  $E_\nu$ :

$$\frac{dN}{dE_\gamma}(E_\gamma, E_\nu) = \frac{m_\nu}{\tau_{\text{cm}}} \frac{1}{E_\nu^2} \left( 1 - \alpha + 2\alpha \frac{E_\gamma}{E_\nu} \right), \quad (12)$$

where  $\tau_{\text{cm}}$  represents the centre-of-mass neutrino lifetime. Taking into account the solar neutrino energy spectrum  $\phi_\nu(E_\nu)$  one can write the expected gamma spectrum in the detector as:

$$\frac{dN}{dE_\gamma}(E_\gamma) = \frac{VT}{c} \int_{E_\gamma}^{E_{\nu, \text{max}}} \frac{dN}{dE_\gamma}(E_\gamma, E_\nu) \phi_\nu(E_\nu) dE_\nu, \quad (13)$$

where  $V$  is the detector volume;  $T$  is time of measurement and  $c$  is the light speed in vacuum.

In the calculations neutrino fluxes given by the Standard Solar Model (SSM) [79] and neutrino energy spectra from [80] were used. The signal shapes (13) were convolved with the detector response function.

The Monte-Carlo method was used in order to simulate the CTF response to gammas. The events were generated according to the spectrum given by (13) inside the inner vessel and in the adjacent water layer of 50 cm. The gamma-electron showers were followed using the EGS-4 code [97].

Taking into account the best ratio of the expected effect to the background, and in order to avoid systematic errors, caused by the uncertainty of the linear part of the background at lower energies, the range 185–380 keV was chosen for the analysis. The maximum likelihood method was used to find the possible contribution from the radiative decay of the SSM solar neutrino in the measured spectrum. The likelihood function was found with the assumption that the number of counts in each channel of the measured spectrum  $S_i^{\text{exp}}$  obeys a normal distribution, and represents the sum of the model function describing the residual background and the spectrum due to the neutrino decay calculated using (6)–(8).

The analysis of the upper limit on the lifetime of the neutrino was performed by minimizing the  $\chi^2(N_0, a, b, \tau_{\text{cm}}/m_\nu)$  value for different values of  $\tau_{\text{cm}}/m_\nu$ . The integration of the probability function gave a value of 0.9 (90% CL) for  $\tau_{\text{cm}}/m_\nu = 4.2 \cdot 10^3 \text{ s} \cdot \text{eV}^{-1}$  ( $\alpha = 0$ ). This limit is practically independent of the lower bound of the analyzed region. The results of the optimal fit for the value  $\tau_{\text{cm}}/m_\nu = 4.2 \cdot 10^3 \text{ s} \cdot \text{eV}^{-1}$  ( $\alpha = 0$ ) are shown in Figs.3,4. In the same way the upper limits  $\tau_{\text{cm}}/m_\nu \geq 1.5 \cdot 10^3 \text{ s} \cdot \text{eV}^{-1}$  ( $\alpha = -1$ ) and  $\tau_{\text{cm}}/m_\nu \geq 9.7 \cdot 10^3 \text{ s} \cdot \text{eV}^{-1}$  ( $\alpha = 1$ ) were obtained. Actually, the analysis of the CTF-II gives a 25% limit on the part of the background in the region of 200–250 keV attributed to the possible neutrino decay. The low sensitivity is explained by a similar behavior of the background and the effect (small negative slope

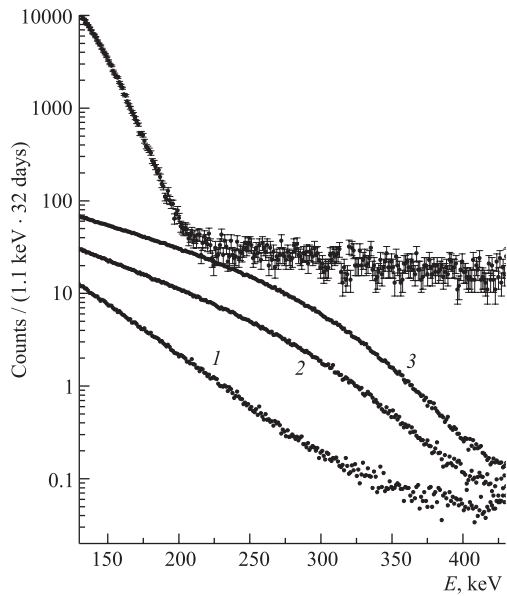


Fig. 3. The experimental spectrum measured by the CTF-II (the upper plot with error bars) and the expected energy spectra of gammas appearing in the radiative decay of the neutrino  $\nu_H \rightarrow \nu_L + \gamma$  calculated by the Monte-Carlo method with  $\tau_{\text{cm}}/m_\nu = 5.0 \cdot 10^3 \text{ s} \cdot \text{eV}^{-1}$  for 3 values of the parameter  $\alpha$ : 1 —  $\alpha = -1$ ; 2 —  $\alpha = 0$ ; 3 —  $\alpha = 1$

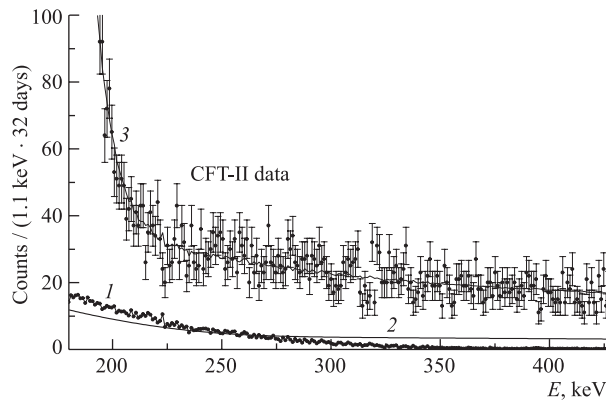


Fig. 4. Fit in the region of 185–380 keV for the radiative neutrino decay and  $\nu_e-e$  scattering due to the charge radius. 1 — Monte-Carlo calculation of the  $\gamma$  signal from the  $\nu_H \rightarrow \nu_L + \gamma$  decay for  $\tau/m_\nu = 4.2 \cdot 10^3 \text{ s} \cdot \text{eV}^{-1}$ ; 2 — spectrum of recoil electrons for the neutrino charge radius  $\langle r^2 \rangle = 2.2 \cdot 10^{-30} \text{ cm}^2$

linear function). In principle, correct modeling of the background can eliminate the major part, which can finally lead to better results. Nevertheless, the obtained values are more than one order of magnitude stronger than those obtained in

reactor and accelerator experiments [89–93], yet still poorer in comparison to the astrophysical considerations [17, 98].

A more stringent indirect limit on the probability of radiative decay can be obtained using the upper bound on the neutrino magnetic moment. On the assumption that  $\mu_{HL}^{\nu} \approx \mu_{\nu} \leq 5.5 \cdot 10^{-10} \mu_B$  and the neutrino mass  $m_{\nu}^2 = 0.35 \text{ eV}$ , one can obtain  $\tau(\nu_2 \rightarrow \nu_1 + \gamma) \geq 1.2 \cdot 10^{29} \text{ s}$  for  $\Delta m_{12}^2 = 6 \cdot 10^{-5} \text{ eV}^2$  and  $\tau(\nu_3 \rightarrow \nu_{1,2} + \gamma) \geq 1.0 \cdot 10^{24} \text{ s}$  for  $\Delta m_{23}^2 = 3 \cdot 10^{-3} \text{ eV}^2$ . These limits are stronger than those obtained using the SN1987A data [17, 18].

### 3. SEARCH FOR THE ELECTRON DECAY MODE $e \rightarrow \gamma + \nu$

The  $U(1)$  gauge invariance of the QED Lagrangian dictates strict conservation of the electric charge and absence of the photon mass. The search for violation of charge conservation (CC) is one of the possible tests when looking for physics beyond the Standard Model. The nonconservation of the electric charge (CNC) can be introduced in the Lagrangian by including additional interactions of leptons with photons in the form  $g(\bar{e}\gamma_{\alpha}\nu + \bar{\nu}\gamma_{\alpha}e)A_{\alpha}$  or with  $Z$  bosons in the form  $G(\bar{\nu}\nu)(\bar{\nu}e)$ . These interactions lead to the decay of the electron  $e \rightarrow \gamma\nu$  or  $e \rightarrow \nu\nu\nu$ . In 1978 Okun, Zeldovich, and Voloshin show that the decay  $e \rightarrow \gamma\nu$  has to be accompanied by emission of a huge number of low energy photons against only one 255.5 keV photon [99, 100]. This is the so-called paradox of the unstable electron. But in the modern view a decaying electron is a paradox too. Detailed discussion can be found in [101], as well as references therein. An additional possibility is connected with the CNC involving interactions with nucleons. Discussions of the CNC in the context of gauge theories can be found in [99–109]. Critical studies of the possible violation of charge conservation have been done both theoretically and experimentally by Okun [106, 107].

**3.1. Experimental Searches for the Violation of Electric Charge Conservation.** Tests of the electric charge conservation in the lepton sector have been performed by studying the following processes:

1. Disappearance or decay of the electron into the invisible channel  $e \rightarrow 3\nu$ . The electron decay is accompanied by the emission of characteristic X rays or Auger electrons due to the transitions of the electrons from higher shells.

2. Decay of the electron into two lightest known detectable particles  $e \rightarrow \nu\gamma$ . The mode can be detected by registering  $\gamma$  quanta with an energy of  $m_e/2$ .

Two other processes include hadrons:

3.  $\beta$  decay without electron emission  $(A, Z) \rightarrow (A, Z+1)^* + \nu_e + \nu_e$ . These decays are searched only for the nuclei with daughter nuclei having nuclear level energies within the energy range of the transition  $Q_0$  to  $Q_0 + m_e$ . The identification of the decay is performed by studying the emission of the daughter nuclei. Another possibility is associated with the search for the daughter nuclei

$(A, Z+1)$  among  $(A, Z)$  nuclei, with the energetically forbidden usual beta-decay and the energetically possible decay without an electron in the final state.

4. Electron capture with violation of the electrical charge  $(A, Z) + e^- \rightarrow (A, Z)^* + \nu_e$ . The search for these processes is performed for the nuclei with low-lying nuclear levels ( $E^* \leq m_e$ ). The identification of the decay is performed by studying the emission of the nuclei of interest.

The first attempt of experimental search for the electron disappearance was made by Feinberg and Goldhaber [110]. They used a 5 kg NaI detector with an energy resolution of 13%. The disappearance of the electron in the inner shell of the I atom should be accompanied by a cascade of X rays and an Auger electrons with a total energy of 33.2 or 5.2 keV corresponding to the electron binding energy in the *K* or *L* shell. As a result, a Gaussian peak should be observed with the half-width corresponding to the detector resolution. The sensitivity of the experiment to the electron lifetime could be estimated using a simple formula in the case when the underlying background spectrum varies slowly in the energy interval comparable with the detector's energy resolution:

$$\tau_{\text{lim}} = \varepsilon N_e \sqrt{\frac{T}{M_d B (3.3\sigma_E)}} \approx \varepsilon 3 \cdot 10^{26} \sqrt{\frac{M_d T}{B (3.3\sigma_E)}}.$$

Here,  $\varepsilon$  is the efficiency of the  $\gamma$ -quanta registering;  $N_e$  is the number of the candidate electrons;  $M_d$  is the mass of the detector (the approximation  $N_e \approx 3 \cdot 10^{26}$  is valid if mass of the detector is measured in kg);  $B$  is the specific background of the detector (the number of counts/(keV · kg · y));  $\sigma_E$  is the detector's energy resolution (the full width at half height FWHM =  $2.36\sigma$ ) and  $T$  is the time of data taking. The limit on the electron lifetime obtained with NaI detectors is  $\tau(e \rightarrow \nu\gamma) \geq 3.5 \cdot 10^{23}$  y. Steinberg was the first to use a germanium detector for the search on the  $e \rightarrow \nu\gamma$  decay [111]. The germanium detector has a much better resolution in comparison with the scintillator detectors, this advantage permitted one to obtain a better limit on the lifetime of the electron  $\tau(e \rightarrow \nu\gamma) \geq 2.1 \cdot 10^{25}$  y using the data collected in experiments on the  $2\beta$  decay [101]. The intrinsic energy resolution of the Ge(Li) or HPGe detectors at 250 keV is as low as  $\simeq 1.5$  keV but the Doppler broadening due to the orbital movement of the electrons results in an increase of the expected width of the  $\gamma$  line, corresponding to the  $e$  decay, up to 5 keV. In Table 2 the experimental limits on the lifetime of the electron in respect to the  $e \rightarrow \nu\gamma$  decay, obtained while searching for  $\gamma$  quanta with an energy  $\approx m_e/2$ , are listed in chronological order. The mass of the detector and the background level at 255 keV are cited for each experiment.

The lowest background level has been achieved with the liquid xenon (LXe) scintillator detector by the DAMA collaboration, their detector being devoted to the dark matter search. The first layer of the passive shielding used in the experiment consisted of oxygen-free electrolytic copper. Oxygen-free copper

Table 2. The limits on the lifetime of the electron in respect of the decay  $e \rightarrow \nu + \gamma$ , obtained while searching for  $\gamma$  quanta with an energy  $\approx m_e/2$

Detector	Mass, kg	Background, (keV · kg · y) <sup>-1</sup>	Limits on $\tau(e \rightarrow \nu + \gamma)$	Year, reference
NaI	5		$1.0 \cdot 10^{19}$ (68%)	1959 [110]
NaI	1.4		$4.0 \cdot 10^{22}$ (68%)	1965 [112]
NaI	6	2300	$3.5 \cdot 10^{23}$ (68%)	1979 [113]
Ge(Li)	0.69	1500	$3.0 \cdot 10^{23}$ (68%)	1983 [114]
HPGe	0.71	240	$1.1 \cdot 10^{25}$ (90%)	1986 [115]
HPGe	3.1	20	$1.2 \cdot 10^{25}$ (90%)	1993 [116]
HPGe	2.2	10	$2.1 \cdot 10^{25}$ (90%)	1995 [117]
LXe	6.5	0.3	$1.0 \cdot 10^{25}$ (90%)	1996 [118]
LXe	6.5	0.06	$2.0 \cdot 10^{26}$ (90%)	2000 [119]
CTF(C <sub>16</sub> H <sub>18</sub> )	4170	0.06	$4.6 \cdot 10^{26}$ (90%)	2002 [120]

and ancient lead free from the radioactive isotope  $^{210}\text{Pb}$  ( $T_{1/2} = 23$  y) have been used as the first layer shielding in many experiments with Ge detectors but the background level achieved in the DAMA experiment is 20 times lower. The relative energy resolution of the LXe detector is  $\sigma_E/E = 0.056 + 1.19\sqrt{E}$ , where energy is measured in keV, the efficiency of the 255 keV  $\gamma$ -quanta registering is 0.85. The total collected data set consists of 2257.7 kg · day and the obtained limit is  $\tau(e \rightarrow \nu\gamma) \geq 2.1 \cdot 10^{25}$  y.

The interaction violating the electric charge conservation can be presented in the same way as a usual weak interaction, replacing the electron with a neutrino:

$$L_{\text{CNC}} = e\varepsilon_{e\nu\gamma} \bar{\psi}_e \gamma_\mu (1 - \gamma_5) \psi_\nu A^\mu + \text{h.c.}$$

In [119] the limit  $\varepsilon_{e\nu\gamma}^2 < 4.3 \cdot 10^{-94}$  at 90% CL was obtained.

The data on the search for the electron decay in the  $e \rightarrow 3\nu$  channel are listed in Table 3. For this decay a more stringent lifetime limit,  $\tau(e \rightarrow 3\nu) \geq 2.4 \cdot 10^{24}$  y, was obtained by the DAMA collaboration with a 95 kg Na(I) detector [121]. The decay mode  $e \rightarrow 3\nu$  is indistinguishable experimentally from the electron disappearance  $e \rightarrow \text{nothing}$  and, hence the upper limit on the lifetime of the electron is valid for the electron disappearance, which is possible in the «world on the brane» models as a transition of the electron from our three-dimensional world to higher dimensions [122, 123].

The probability of the electric charge nonconserving decay (CNC)  $e \rightarrow \nu\nu\nu$  can be presented in the form  $T_{e3\nu}^{\text{CNC}} = \varepsilon_{e3\nu}^2 T_\mu^{\text{CC}} f_e/f_\mu$ , where  $T_\mu^{\text{CC}}$  is the probability of the muon decay  $\mu \rightarrow e + \nu_e + \nu_\mu$ , and  $f_e/f_\mu$  is the ratio of the phase-space factors for the electron and muon decays [125]. The limit obtained in [121]

for the electron lifetime  $\tau(e \rightarrow 3\nu) \geq 2.4 \cdot 10^{24}$  y corresponds to the limit  $\varepsilon_{e3\nu}^2 \leq 1.1 \cdot 10^{-27}$  (90% CL).

**Table 3. Limits on the lifetime of the electron in respect of the decay  $e \rightarrow 3\nu$ , obtained while searching for the characteristic X rays and Auger electrons**

Detector	Mass, kg	Limits on $\tau(e \rightarrow \nu\nu\nu)$	Year, reference
NaI	5	$1.0 \cdot 10^{18}$ (68%)	1959 [110]
NaI	1.4	$2.0 \cdot 10^{21}$ (68%)	1965 [112]
Ge(Li)	0.35	$5.3 \cdot 10^{21}$ (68%)	1975 [111]
NaI	6	$2.0 \cdot 10^{22}$ (68%)	1979 [113]
Ge(Li)	0.69	$2.0 \cdot 10^{22}$ (68%)	1983 [114]
HPGe	2.2	$1.7 \cdot 10^{23}$ (90%)	1986 [124]
NaI	722	$1.2 \cdot 10^{23}$ (90%)	1993 [109]
HPGe	2.2	$2.6 \cdot 10^{23}$ (90%)	1995 [117]
LXe	6.5	$1.5 \cdot 10^{23}$ (90%)	1996 [118]
NaI	95	$2.4 \cdot 10^{24}$ (90%)	2000 [121]

The possible mechanisms of the charge violating interaction with participation of nucleons were considered in [125, 126]. The first experiment on the search for the electric charge nonconservation in the processes involving nucleons was performed on the  $^{87}\text{Rb}$  nucleus. The  $\beta$  decay of the  $^{87}\text{Rb}$  nucleus has an endpoint energy of 273 keV and a lifetime of the transition to the  $^{87}\text{Sr}$  ground state of  $4.8 \cdot 10^{10}$  y. At the same time, the decay  $^{87}\text{Rb} \rightarrow ^{87}\text{Sr}$  without the emission of electrons is energetically allowed for the transition into the 388 keV excited state. For another couple of nuclei,  $^{71}\text{Ga}$  and  $^{71}\text{Ge}$ , the usual  $\beta$  decay is forbidden but the value  $Q < m_e$  energetically allows the transition  $^{71}\text{Ga} \rightarrow ^{71}\text{Ge}$  without electron in the final state. A more stringent limit for the processes  $(A, Z) \rightarrow (A, Z + 1)^* + \nu_e + \nu_e$  was obtained from the data of the Ga–Ge solar neutrino detector Gallex:  $\tau \geq 3.5 \cdot 10^{26}$  y. The results of other experiments are compiled in Table 4. The ratio of the probability of a charge nonconserving interaction to the probability of a usual weak interaction is  $\varepsilon_W^2 = \Gamma(n \rightarrow p + \nu_e + \nu_e) / \Gamma(n \rightarrow p + \nu_e + \nu_e) \leq 8 \cdot 10^{-27}$  [127].

The electron capture with violation of the electric charge conservation giving an excited nucleus in the final state is possible for the nuclei with low-lying nuclear levels. The process can occur both due to the exchange of  $W$  and  $Z$  bosons, and due to the exchange of the photon. The search for the transitions  $(A, Z) + e^- \rightarrow (A, Z)^* + \nu_e$  was performed for the nuclei  $^{127}\text{I}$ ,  $^{23}\text{Na}$ , and  $^{129}\text{Xe}$  with the NaI and LXe detectors, respectively (Table 5).

Table 4. Limits on the lifetime of the nucleus  $(A, Z)$  in respect of the CNC decay  $(A, Z) \rightarrow (A, Z + 1)^* + \nu_e + \nu_e$  (from [133])

Decay	Mass, kg	Limits on $\tau$ , y	Year, reference
$^{87}\text{Rb} \rightarrow ^{87m}\text{Sr}$	0.03	$1.8 \cdot 10^{16}$ (90%)	1960 [128]
$^{87}\text{Rb} \rightarrow ^{87m}\text{Sr}$	0.4	$1.9 \cdot 10^{18}$ (90%)	1979 [129]
$^{71}\text{Ga} \rightarrow ^{71}\text{Ge}$	300	$2.3 \cdot 10^{23}$ (90%)	1980 [130]
$^{87}\text{Rb} \rightarrow ^{87m}\text{Sr}$	0.8	$7.5 \cdot 10^{19}$ (90%)	1983 [131]
$^{113}\text{Cd} \rightarrow ^{113m}\text{In}$	1.5	$1.4 \cdot 10^{18}$ (68%)	1983 [132]
$^{71}\text{Ga} \rightarrow ^{71}\text{Ge}$	60000	$3.5 \cdot 10^{26}$ (90%)	1986 [127]
$^{73}\text{Ge} \rightarrow ^{73}\text{As}$	0.95	$2.6 \cdot 10^{23}$ (90%)	1993 [133]

Table 5. Limits on the lifetime of the nucleus  $(A, Z)$  in respect of the CNC electron capture  $(A, Z) + e^- \rightarrow (A, Z)^* + \nu_e$

Decay	Mass, kg	Limits on $\tau$ , y	Year, reference
$^{127}\text{I} \rightarrow ^{127}\text{I}^*$	40	$2.1 \cdot 10^{21}$ (90%)	1987 [126]
$^{127}\text{I} \rightarrow ^{127}\text{I}^*$	900	$6.0 \cdot 10^{22}$ (90%)	1991 [125]
$^{127}\text{I} \rightarrow ^{127}\text{I}^*$	87	$2.4 \cdot 10^{23}$ (90%)	1999 [135]
$^{23}\text{Na} \rightarrow ^{23}\text{Na}^*$	87	$1.5 \cdot 10^{23}$ (90%)	1999 [135]
$^{129}\text{Xe} \rightarrow ^{129}\text{Xe}^*$	6.5	$(1-4) \cdot 10^{24}$ (90%)	1983 [134]

Let us use the notation  $\varepsilon_W$  and  $\varepsilon_\gamma$  for the ratio of the probability of the charge nonconserving interaction to the probability of the interaction leading to the usual electron capture  $G_W^{\text{CNC}} = \varepsilon_W G_F$  or to the emission of conversion electrons in the  $\gamma$  transitions  $G_\gamma^{\text{CNC}} = \varepsilon_\gamma \alpha$ . The limits for these parameters, obtained from the experiments on the search for the reaction  $(A, Z) + e^- \rightarrow (A, Z)^* + \nu_e$ , are  $\varepsilon_W^2 \leq 2.2 \cdot 10^{-26}$  and  $\varepsilon_\gamma^2 \leq 1.3 \cdot 10^{-42}$  [109, 134].

In such a way, it is experimentally confirmed that the lifetime of electrons and nuclei with respect to the electric charge nonconserving decays is longer than  $10^{24}$ – $10^{26}$  y. The probabilities of these processes with respect to the probabilities of the charge conserving decays caused by the weak interaction, namely, the usual  $\beta$  decay, electron capture and muon decay, are less than  $(\varepsilon_W^\beta)^2 \leq 8 \cdot 10^{-27}$ ,  $(\varepsilon_W)^2 \leq 2.2 \cdot 10^{-26}$  and  $(\varepsilon_W^{3\nu})^2 \leq 1.1 \cdot 10^{-27}$ , respectively. The processes caused by the electromagnetic interactions are suppressed by  $(\varepsilon_\gamma^{\text{IC}})^2 \leq 1.3 \cdot 10^{-42}$  for the emission of conversion electrons, and by  $(\varepsilon_{\nu\gamma})^2 \leq 4.3 \cdot 10^{-94}$  for the vertex with photons.

**3.2. Limits on the Electron Decay Mode  $e \rightarrow \nu + \gamma$  with the Prototype of the Borexino Detector.** The search for the electron decay  $e \rightarrow \nu + \gamma$  is possible only with a detector on the base of a liquid organic scintillator. The binding

energy of the electron in the carbon atom is only 283 eV, which is too low to be registered, hence the search for the decay mode  $e \rightarrow 3\nu$  is impossible. The mass difference of the nuclei  $^{12}\text{C}$  and  $^{12}\text{N}$  of 17 MeV energetically forbids the  $\beta$  decay without the emission of the electron  $(A, Z) \rightarrow (A, Z + 1)^* + \nu_e + \nu_e$ . Likewise, the energy of the first excited state of the  $^{12}\text{C}$  nucleus, 4.4 MeV, is too high for the process  $(A, Z) + e^- \rightarrow (A, Z)^* + \nu_e$ . As it was noticed above, the CTF detector has an extremely low background level at an energy of 250 keV and comparatively big mass (4.2 t). This permitted one to obtain the best sensitivity with respect to the  $e \rightarrow \nu\gamma$  decay mode.

The Monte-Carlo method has been used in order to simulate the CTF response to the 256 keV gamma. The hypothetical electron decay can occur both in the scintillator and in water. The decays in the scintillator and water were simulated separately and then summed taking into account the number of the candidate electrons (Fig. 5). The response function was normalized to one electron decay in the scintillator volume. The limit on the lifetime was calculated by the formula

$$\tau \geq \varepsilon N_e T / S_{\text{lim}}, \quad (14)$$

where  $N_e = 1.36 \cdot 10^{30}$  is the number of electrons inside the scintillator;  $T = 32.1$  days is the time of measurement;  $S_{\text{lim}} = 170$  is the upper limit on the number of counts of response function inside the fitting interval;  $\varepsilon = 0.67$  is the fraction of the events left after a spatial cut applied. The last value was

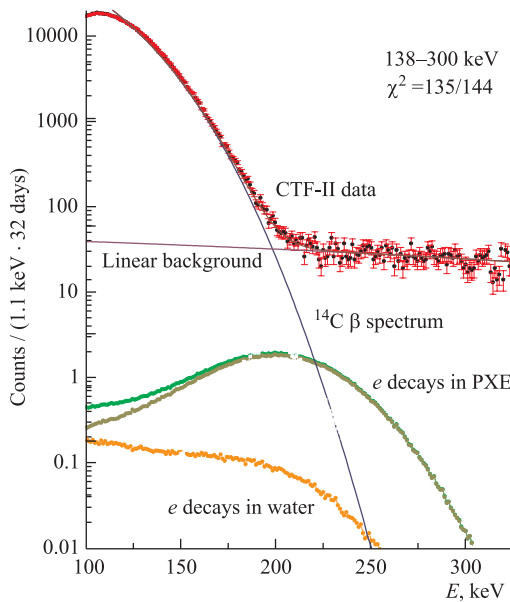


Fig. 5. CTF spectrum with a superimposed fit curve and results of 256 keV  $\gamma$  Monte-Carlo simulations. The Monte-Carlo results are normalized to 170 electron decay events in the inner vessel. Additional gammas, arriving from the decays in the surrounding water, are shown as well. The total detector's response to the 256 keV  $\gamma$  is the sum of the gammas from scintillator PXE and water surrounding the inner vessel with PXE

estimated from the number of  $^{14}\text{C}$  events lost in the region around 150 keV after the spatial cut. Analysis of the likelihood function gives the value  $S \leq 170$  decays at 90% CL. The likelihood function for  $S = 0$  reaches its maximum at  $\alpha = -0.72$ , and for  $S = 170$  at  $\alpha = -0.8$ . As a result, a new lower limit on the mean lifetime for the decay  $e \rightarrow \gamma + \nu$  has been established  $\tau \geq 4.6 \cdot 10^{26}$  y (90% CL) [120]. The limit is 2.3 times stronger than the previous DAMA result.

#### 4. EXPERIMENTAL LIMITS ON THE VIOLATION OF THE PAULI EXCLUSION PRINCIPLE

The Pauli exclusion principle (PEP) is the basis for the describing of the structure and properties of atoms and atomic nuclei composed of fermions. The exclusion principle was formulated by W. Pauli in 1925 and in its original form postulated that only one electron with a definite spin orientation could occupy each of the allowed Bohr's orbits in an atom. In such a way the PEP explained the regularities of the Periodic Table and atomic spectra. In the modern Quantum Field Theory (QFT) the PEP appears automatically for a system of identical fermions as a result of the anticommutativity of the fermion creation and annihilation operators. Violation of the PEP as well as of the electric charge nonconservation contradicts the modern quantum field theory.

The PEP is of fundamental importance but its tests were started extensively in direct experiments 15 years later than the tests of the electron stability. Goldhaber pointed out that the same experimental data which had been used to set a limit on the lifetime of the electron could be used to test the validity of the PEP for atomic electrons [136]. Pioneering experiments were performed by Reines and Sobel by searching for X rays emitted in a transition of an  $L$ -shell electron to the filled  $K$  shell in an atom [136], and by Logan and Lubicic who searched for  $\gamma$  quanta emitted in a forbidden by the PEP transition of the nucleon in the  $^{12}\text{C}$  nucleus [137]. In 1980 Amado and Primakoff pointed out that in the framework of the QFT these PEP-forbidden transitions could not take place even in the case of a PEP violation [138]. Later a theoretical framework describing a small violation of the PEP was constructed in [139–141] but it was found that even small PEP violations lead to negative probabilities for some processes [142]. Critical studies of the possible violation of PEP have been done both theoretically and experimentally by Okun [106, 107].

One of the possibilities to test the PEP violation is the search for atoms or nuclei in a non-Paulian state, another is the search for the prompt radiation accompanying non-Paulian transitions.

Violation of the PEP in the nucleon system has been studied by searching for the non-Paulian transitions with  $\gamma$ - [137, 143, 144],  $p$ - [145, 146] and  $n$ - [147]

emission, non-Paulian  $\beta^+$ ,  $\beta^-$  decays [144,148] as well as in nuclear  $(p, p)$ ,  $(p, \alpha)$  reactions on  $^{12}\text{C}$  [149].

**4.1. Search for Prompt Radiation Accompanying Non-Paulian Transitions with the CTF.** The non-Paulian transitions were searched for the nuclei  $^{12}\text{C}$  and  $^{16}\text{O}$  contained in the sensitive volume of scintillator and in the water shield of the CTF-II detector [150]. The scheme of nucleon level of the  $^{12}\text{C}$  nuclei is shown in Fig.6. The transition of the nucleon from the  $P$  shell to the filled  $S$  shell will result in the excited  $^{12}\text{C}$  nuclei. The excitation energy corresponds to the difference of the binding energies of nucleons on the  $S$  and  $P$  shell. The nucleon binding

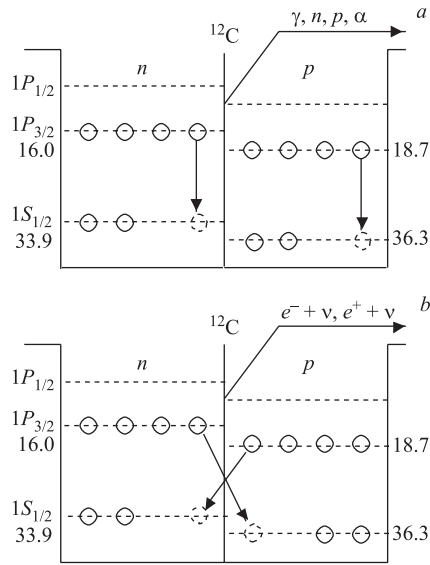


Fig. 6. Population of the energy levels with protons and neutrons for the  $^{12}\text{C}$  ground state in a simple shell model (energy in MeV units). Schemes of non-Paulian transitions of nucleons from the  $P$  shell to the filled  $S$  shell: a) with  $\gamma$ -,  $n$ -,  $p$ - and  $\alpha$  emission; b) with  $\beta^+$ -,  $\beta^-$  emission

ratio and spectra of particles were considered in [153]. The values of  $E_{1S_{1/2}}$  from Table 6 were used for the approximate calculation of the binding energy of the non-Paulian nuclei and  $Q$  value of the reaction. Weak processes with violation of the PEP ( $\beta^+$ ,  $\beta^-$  decays) [144,148] with a non-Paulian nucleon in the final state (on the  $1S_{1/2}$  shell) were considered as well.

energies for the light nuclei  $^{12}\text{C}$ ,  $^{16}\text{O}$  were measured while studying  $(p, 2p)$  and  $(p, np)$  proton scattering reactions with an energy of 1 GeV [151]. The measured values are  $E_n(1S_{1/2}, ^{12}\text{C}) = 36.3 \pm 0.6$  MeV and  $E_p(1S_{1/2}, ^{12}\text{C}) = 33.9 \pm 0.9$  MeV. One can compare the obtained data with those on the  $(e, e'p)$  scattering, which give a significantly different value of  $E_p(1S_{1/2}, ^{12}\text{C}) = 39 \pm 1$ . Table 6 shows the values of  $E_{S_{1/2}}$  which are closer to the nucleon separation energy  $S_n, S_p$  [152]. As one can see from the Table, the energy release in the non-Paulian transitions in  $^{12}\text{C}$  and  $^{16}\text{O}$  is comparable with the energies  $S_p, S_n, S_\alpha$ , hence together with the emission of  $\gamma$  quanta, the emission of  $n, p$  and  $\alpha$  is possible.

Because of the existing significant discrepancy in the values of  $E_{S_{1/2}}^{n,p}$ , prediction of the branching ratio for the emission in each of the above-mentioned channels is a very complicated task. For the case of the nucleon and dinucleon decay in nuclei, the branching ratio

Table 6. The separation energy  $S_p$ ,  $S_n$ ,  $S_\alpha$  (MeV) [152], the nucleon energy (with errors) of the  $1P_{3/2}$  and  $1S_{1/2}$  shells (MeV) [151], and the nuclear binding energy  $E_b$  (keV) [152]

	$^9\text{Be}$	$^{11}\text{B}$	$^{12}\text{C}$	$^{16}\text{O}$
$S_p$	16.9	11.2	16.0	12.3
$S_n$	1.66	10.7	18.7	15.7
$S_\alpha$	2.5	8.7	7.4	7.2
$1P_{3/2}(p)$	17.0 (0.2)	17.5 (0.5)	16.0 (0.2)	18.0 (0.3)
$1P_{3/2}(n)$	18.1 (0.5)	18.4 (0.6)	19.0 (0.3)	22.0 (0.4)
$1S_{1/2}(p)$	27.7 (0.5)	33.5 (0.9)	33.9 (0.9)	39.8 (0.9)
$1S_{1/2}(n)$	29.2 (0.8)	34.5 (1.0)	36.3 (0.6)	42.2 (1.0)
$E_b$	58164.9	76204.8	92161.8	127619.3

**4.2. Limits on the Non-Paulian Transitions in  $^{12}\text{C}$  and  $^{16}\text{O}$  with Emission of  $\gamma$ ,  $p$ ,  $\alpha$ , and  $n$ .** As follows from Table 6, the energy difference for the nucleon transition from the shell  $1P_{3/2}$  to the shell  $1S_{1/2}$  is  $\approx 17.5$  MeV for  $^{12}\text{C}$ . The response functions of the CTF-II to the gamma of this energy were simulated by MC method described in the previous subsection. The energy difference for the same transition in the case of  $^{16}\text{O}$  corresponds to  $\approx 21$  MeV. The uniformly distributed gammas of this energy were simulated in a 1 m thick layer of water surrounding the scintillator. Both the response functions are shown in Fig. 7 before and after the muon veto suppression. High energy release in the liquid scintillator can activate the muon veto of the CTF, resulting in the rejection of the event. Probability of identification of an event with higher energy in the scintillator by the muon veto has been specially studied [154]. High energy release in the liquid scintillator can activate the muon veto of the CTF-II, resulting in the rejection of the event.

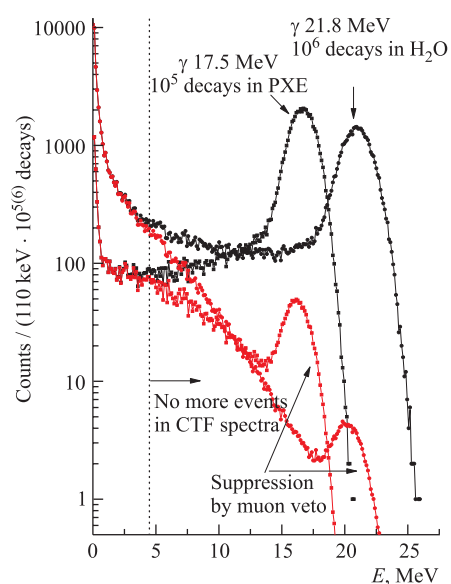


Fig. 7. Expected response functions of the detector for the  $^{12}\text{C} \rightarrow ^{12}\tilde{\text{C}} + \gamma$  decays in the liquid scintillator and the  $^{16}\text{O} \rightarrow ^{16}\tilde{\text{O}} + \gamma$  decays in the water shield before and after the muon veto suppression

The limit on the probability of the transitions  $^{12}\text{C} \rightarrow ^{12}\tilde{\text{C}} + \gamma$  and  $^{16}\text{O} \rightarrow ^{16}\tilde{\text{O}} + \gamma$  violating the PEP are based on the experimental fact of observing no events with an energy higher than 4.5 MeV not accompanied by the muon veto signal. The lower limit on the PEP violating transitions of nucleons from the  $P$  shell to the occupied  $1S_{1/2}$  shell was obtained using the formula:

$$\tau \geq \varepsilon_{\Delta E} N_N N_n T / S_{\text{lim}}, \quad (15)$$

where  $\varepsilon_{\Delta E}$  is the efficiency of registering an event in the energy interval  $\Delta E$ ;  $N_N$  is the number of nuclei under consideration;  $N_n$  is the number of nucleons ( $n$  and/or  $p$ ) in the nuclei for which non-Paulian transitions are possible;  $T$  is the total time of measurements, and  $S_{\text{lim}}$  is the upper limit on the number of candidate events registered in the  $\Delta E$  energy interval and corresponding to the chosen confidence level.

The energy released in the transition  $^{12}\text{C} \rightarrow ^{11}\tilde{\text{B}} + p$  is the difference between the binding energies of the final and initial nuclei. Using evident notations one can write:

$$Q(^{12}\text{C} \rightarrow ^{11}\tilde{\text{B}} + p) = M(^{12}\text{C}) - M(^{11}\tilde{\text{B}}) - m_p = -E_b(^{12}\text{C}) + E_b(^{11}\tilde{\text{B}}). \quad (16)$$

The binding energy of the non-Paulian nuclei with 3 neutrons  $E_b(^{11}\tilde{\text{B}}_n)$  or 3 protons  $E_b(^{11}\tilde{\text{B}}_p)$  on the  $S$  shell can be evaluated by considering the binding energy  $E_b(^{11}\text{B})$  and the difference between the binding energies of nucleons on the  $S$  shell  $E_{n,p}(S_{1/2})$  and the binding energy of the last nucleon  $S_{n,p}(^{11}\text{B})$ :

$$E_b(^{11}\tilde{\text{B}}_{n,p}) \simeq E_b(^{11}\text{B}) + E_{n,p}(1S_{1/2}) - S_{n,p}(^{11}\text{B}). \quad (17)$$

Using the data of Table 6, one can obtain  $Q(^{12}\text{C} \rightarrow ^{11}\tilde{\text{B}}_p + p) = 6.3$  MeV and  $Q(^{12}\text{C} \rightarrow ^{11}\tilde{\text{B}}_n + p) = 7.8$  MeV. Taking into account the recoil energy of the nuclei and experimental errors of  $E_{n,p}(S_{1/2})$  from Table 6, the energy of a proton released in these non-Paulian transitions is  $E_p = 5.8(7.2) \pm 1.0$  MeV.

The light yield for the protons in the range 0.6–6.0 MeV was measured for the NE213 scintillator using recoil protons from the  $(n, p)$  elastic scattering [156]. The light yield for a proton with the energy  $E_p = 5.8(7.2)$  MeV corresponds to the electron energy  $E_e = 2.8(3.9) \pm 0.5$  MeV. It means that the proton peak can be found in the energy interval 2.0–4.7 MeV with 90% probability. The binding energy of an  $\alpha$  particle in the  $^{12}\text{C}$  nuclei is as low as 7.4 MeV. The energy released in the transition is the difference between the binding energies of the final and initial nuclei:

$$Q(^{12}\text{C} \rightarrow ^8\tilde{\text{Be}} + \alpha) = -E_b(^{12}\text{C}) + E_b(^8\tilde{\text{Be}}) + E_b(^4\text{He}). \quad (18)$$

The  $\alpha$  particles from the decay can be found in the energy interval 1.0–3.0 MeV with 90% probability. In accordance with the data of [156], the light

yield for an  $\alpha$  with energies 1.0–3.0 MeV corresponds to an electron in the energy range 70–230 keV. The results on the electron stability, obtained on the same experimental data, can be used to set strong limits on the peak if it is situated near the end-point of  $\beta$  spectrum [120]. For  $\alpha$  particles with the lower energy  $E_\alpha = 1$  MeV ( $E_e = 70$  keV) the limit is essentially weaker.

$$\tau(^{12}\text{C} \rightarrow {}^8\tilde{\text{Be}} + \alpha) \geq 6.1 \cdot 10^{23} \text{ y (90\% CL)}. \quad (19)$$

The energy released in the decay  $^{12}\text{C} \rightarrow {}^{11}\tilde{\text{C}} + n$  is equal to the difference between the binding energies of  $^{12}\text{C}$  and  ${}^{11}\tilde{\text{C}}$ . The resulting neutrons are thermalized in hydrogen-rich media (an organic scintillator or water). The lifetime of the neutrons in water and/or scintillator is the order of some hundreds  $\mu\text{s}$ , after which the neutrons are captured by protons with emission of the  $\gamma$ 's with 2.2 MeV energy.

The response function of the CTF-II to the gammas of 2.2 MeV was obtained using the MC model. The response function for  $10^6$  initial gammas generated in the liquid scintillator volume, and for  $10^7$  gammas generated in a water layer of 100 cm, are shown in Fig. 7. The response functions correspond to practically equal probabilities of the non-Paulian transitions for nucleons in the  $^{12}\text{C}$  and  $^{16}\text{O}$  nuclei. The total number of captured neutrons in the CTF-II can be limited to  $N \leq 2.7 n/(d \cdot t)$ . This value is close to the expected rate of neutron production by muons  $N \approx 1 n/(d \cdot t)$  [157].

**4.3. Limits on the Non-Paulian  $\beta^\pm$  Transitions in  $^{12}\text{C}$ .** The nucleus  $^{12}\text{N}$  is unstable; it decays via  $^{12}\text{N} \rightarrow ^{12}\text{C} + e^+ + \bar{\nu}$  with the energy release  $Q = 17.3$  MeV. The inverse process  $^{12}\text{C} \rightarrow ^{12}\tilde{\text{N}} + e^- + \bar{\nu}$  is possible if the binding energy of the non-Paulian nucleus  $E_b(^{12}\tilde{\text{N}})$  is increased in comparison to the binding energy of the normal  $^{12}\text{N}$  nucleus by a value exceeding  $Q$ . The energy released in the reaction  $^{12}\text{C} \rightarrow ^{12}\tilde{\text{N}} + e^- + \bar{\nu}$  is

$$Q = m_n - m_p - m_e - E_b(^{12}\text{C}) + E_b(^{12}\tilde{\text{N}}). \quad (20)$$

The value of  $E_b(^{12}\tilde{\text{N}})$  can be approximated by  $E_b(^{12}\tilde{\text{N}}) \simeq E_b(^{12}\text{N}) + E_p(S_{1/2}, ^{12}\text{N}) - S_p(^{12}\text{N})$ . The separation energy of the proton in  $^{12}\text{N}$  has a very low value,  $S_p(^{12}\text{N}) = 0.6$  MeV. The value of  $E_p(S_{1/2}, ^{12}\text{N})$  can be approximated by the mean value of the binding energies on the  $S_{1/2}$  shell for two neighboring nuclei  $E_p(S_{1/2}, ^{12}\text{N}) \simeq 0.5 \cdot (E_p(S_{1/2}, ^{12}\text{C}) + E_p(S_{1/2}, ^{16}\text{O})) = 36.8$  MeV. Hence the value of  $Q$  is 18.9 MeV. The energy release for the reaction  $^{12}\text{C} \rightarrow ^{12}\tilde{\text{B}} + e^+ + \nu$ , calculated in the same way,  $Q = 17.8$  MeV.

The limits on the probability of these transitions are based on the fact of observing no events with  $E_e \geq 4.5$  MeV nonaccompanied by a muon veto signal. The probability  $\eta(E_e)$  of the muon veto triggering for the high energy events in the scintillator has been taken into account (Fig. 8).

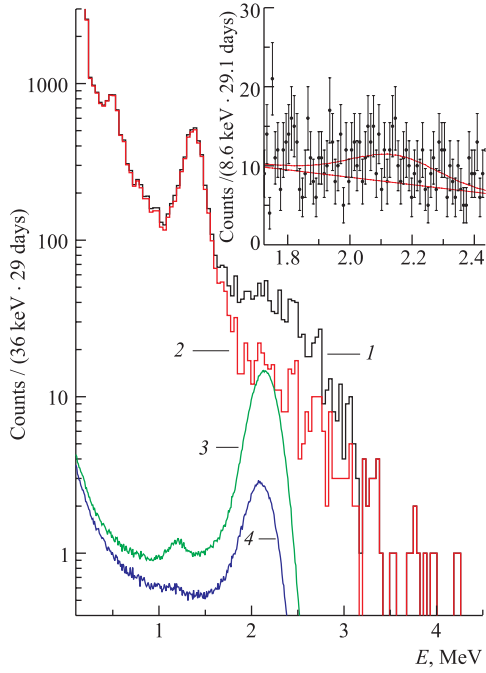


Fig. 8. Background energy spectra of the 4.2 t Borexino CTF-II detector measured during 29 days: 1 — with muon veto, radial cut ( $R \leq 100$  cm) and  $\alpha/\beta$  discrimination applied; 2 — pairs of correlated events (with the time interval  $\Delta t \leq 8.2$  ms between signals) are removed; 3 — the expected response functions of the detector for  $\gamma$  with energy 2.2 MeV due to  $(n, p)$  capture in the scintillator and 4 — in the water. Corresponding mean lifetime for the  $^{12}\text{C} \rightarrow ^{11}\tilde{\text{C}} + n$  and  $^{16}\text{O} \rightarrow ^{15}\tilde{\text{O}} + n$  is  $\tau_{\text{lim}} = 4.1 \cdot 10^{26}$  y. In the inset the fit curve in the energy interval 1.7–2.5 MeV is shown

Table 7. Mean lifetime limits,  $\tau_{\text{lim}}$  (at 90% CL), for non-Paulian transitions in the CTF

Channel	$E_0$ , MeV	$\Delta E$ , MeV	$\tau_{\text{lim}}$ , y (90% CL)	Previous limits
$^{12}\text{C} \rightarrow ^{12}\tilde{\text{C}} + \gamma$	17.5	$\geq 4.5$	$2.1 \cdot 10^{27}$	$4.2 \cdot 10^{24}$ [144]
$^{16}\text{O} \rightarrow ^{16}\tilde{\text{O}} + \gamma$	21.8	$\geq 4.5$	$2.1 \cdot 10^{27}$	$2.7 \cdot 10^{27}$ [143]
$^{12}\text{C} \rightarrow ^{11}\tilde{\text{B}} + p$	4.8–8.2	2.0–4.7	$5.0 \cdot 10^{26}$	$1.7 \cdot 10^{25}$ [145]
$^{12}\text{C}(^{16}\text{O}) \rightarrow ^{11}\tilde{\text{C}}(^{15}\tilde{\text{O}}) + n$	2.2	1.7–2.5	$3.7 \cdot 10^{26}$	$1.0 \cdot 10^{20}$ [147]
$^{12}\text{C} \rightarrow ^8\tilde{\text{Be}} + \alpha$	2.0	0.07–0.23	$6.1 \cdot 10^{23}$	—
$^{12}\text{C} \rightarrow ^{12}\tilde{\text{N}} + e^- + \bar{\nu}_e$	18.9	$\geq 4.5$	$7.6 \cdot 10^{27}$	$3.1 \cdot 10^{24}$ [144] $\sim 8 \cdot 10^{27}$ [155]
$^{12}\text{C} \rightarrow ^{12}\tilde{\text{B}} + e^+ + \nu_e$	17.8	$\geq 4.5$	$7.7 \cdot 10^{27}$	$2.6 \cdot 10^{24}$ [144]

Note.  $E_0$  is the average energy of particles, or end-point energy in the case of  $\beta^\pm$  transitions;  $\Delta E$  is the energy window of the CTF where decays were searched for;  $\varepsilon_{\Delta E}$  is the detection efficiency;  $S_{\text{lim}}$  is the excluded number of events in the CTF spectrum.

The final results for the PEP violation transitions are shown in Table 7 in comparison with the previous results. Comparing these values with the data of Table 7, one can see that these limits for the non-Paulian transitions in  $^{12}\text{C}$  with

$\gamma$ -,  $p$ -,  $n$ -, and  $\alpha$  emissions are the best to date limits. The limits on the  $\beta^\pm$  non-Paulian transitions in  $^{12}\text{C}$  are comparable with those that can be obtained with the data of the LSD detector [148, 155], and the limit on the non-Paulian transition in  $^{16}\text{O}$  with  $\gamma$  emission is comparable with the result obtained using the Kamiokande data [143].

## 5. LIMITS ON THE NUCLEON DECAYS INTO INVISIBLE CHANNELS

The baryon ( $B$ ) and lepton ( $L$ ) numbers are considered to be conserved in the SM. However, no symmetry principle underlies these laws, such as, e.g., gauge invariance, which guarantees conservation of the electric charge. Many extensions of the SM include  $B$  and  $L$  violating interactions, predicting processes with  $\Delta B = 1, 2$  and  $\Delta(B-L) = 0, 2$  leading to the decay of protons and neutrons bounded in the nucleus [158–161]. Despite the extensive experimental studies, no evidence for nucleon instability has been found to date. Most of the studies have been devoted mainly to nucleon decays into strongly or electromagnetically interacting particles. The experimental limits are established for 70 different modes of the proton decay into leptons, mesons, and photons. The value of the lower limits on the nucleon mean lifetime for the majority of the decay modes is  $10^{30}$ – $10^{33}$  y. The stringent limit  $\tau_p \geq 5 \cdot 10^{33}$  y has been obtained for the decay mode  $p \rightarrow e^+ + \pi^0$ .

At the same time, for modes where nucleons disappear or decay to some weakly interacting particles (neutrinos, majorons, etc.), the experimental bounds are 5–6 orders of magnitude lower. Nucleon decays into 3 and more leptons were considered in [162], dinucleon state decays into 2 leptons were studied in [163]. A process with the violation of the lepton number in which two neutrons in the nucleus disappear emitting a majoron,  $nn \rightarrow \chi$ , was considered in [164], the expected lifetime being  $\tau_{nn} 10^{32}$ – $10^{39}$  y. Disappearance of the particles from our «world on the brane» with 3 spatial dimensions (the decays  $N, NN \rightarrow$  nothing) could be an argument for the theories with additional dimensions [165]. The lifetime of the proton with respect to the transitions into extra-dimensions calculated in [166] is  $\tau \sim 10^{35}$  y. The experimental methods of the search for the decays into the «invisible» channel and/or obtaining the upper limits on the probability of such processes could be subdivided into:

1. Spontaneous nuclear fission under the assumption that the nucleon decay will result in the fission of the nucleus. Spontaneous fission of the  $^{232}\text{Th}$  nucleus was discovered by Flerov [167], the lifetime of its spontaneous nuclear fission gives the lower bound on the lifetime of the proton  $\tau_p \geq 1.2 \cdot 10^{23}$  y, and the neutron  $\tau_n \geq 1.8 \cdot 10^{23}$  y. These limits are valid for any mode of the nucleon decay including the «invisible» channel.

2. Search for free neutrons created after a proton decay or disappearance in the deuterium nucleus. The SNO is the most sensitive to this process detector [168]. The limit obtained by Zdesenko and Tretyak for the proton lifetime in respect to the decay into the «invisible» channel is  $\tau_p \geq 3.5 \cdot 10^{28}$  y [169,170].

3. Geochemical or radiochemical search for daughter nuclides appearing after a nucleon decay in the parent nuclei. This method, suggested by Evans and Steinberg [171], is independent of the decay mode. The decay of the neutron or proton in the  $^{130}\text{Te}$  nucleus should lead to the creation of  $^{129}\text{Xe}$  in the sequential decays  $(n) \ ^{130}\text{Te} \rightarrow ^{129}\text{Te} \rightarrow ^{129}\text{I} \rightarrow ^{129}\text{Xe}$  or  $(p) \ ^{130}\text{Te} \rightarrow ^{129}\text{Sb} \rightarrow ^{129}\text{Te} \rightarrow ^{129}\text{I} \rightarrow ^{129}\text{Xe}$ . The measured concentrations of the xenon isotope in tellurium samples give the following limits:  $\tau_p \geq 7.4 \cdot 10^{24}$  y, and  $\tau_n \geq 8.6 \cdot 10^{24}$  y [171]. Search for  $^{37}\text{Ar}$ , appearing in the decay of nucleons in the  $^{39}\text{Ar}$  nucleus, gives the following limits:  $\tau_{p,n} \geq 1.1 \cdot 10^{26}$  y [172, 173],  $\tau_{nn} \geq 4.2 \cdot 10^{25}$  y and  $\tau_{np} \geq 2.1 \cdot 10^{25}$  y [174].

4. Search for prompt  $\gamma$  quanta emitted by a nucleus in a deexcitation process after nucleon decays within the inner nuclear shell. The search for the  $\gamma$  quanta with the energy in the interval 19–50 MeV, which should appear in the decay of a neutron in the inner shell of  $^{16}\text{O}$ , performed with the Kamiokande detector, gives the limit  $\tau_n \geq 4.9 \cdot 10^{26}$  y [175]. Recently, more stringent limits have been obtained with the SNO while searching for the  $\gamma$  quanta with the energy of 6–7 MeV:  $\tau_n \geq 1.9 \cdot 10^{29}$  y, and  $\tau_p \geq 2.1 \cdot 10^{29}$  y [176].

5. Detection of neutrinos from the nucleon decays  $N \rightarrow 3\nu$  and  $NN \rightarrow 2\nu$  within the Earth. In 1979 Learned, Reines, and Soni [177] obtained a limit on the lifetime of the neutron  $\tau(n \rightarrow 3\nu_\mu) \geq 5.0 \cdot 10^{26}$  y from the data of the large volume scintillator detector. The search for the geo-neutrinos performed with the 900 t iron detector Frejus, gave the following results:  $\tau(n \rightarrow 3\nu_\mu) \geq 1.2 \cdot 10^{26}$  y,  $\tau(n \rightarrow 3\nu_e) \geq 3.0 \cdot 10^{25}$  y,  $\tau(nn \rightarrow 2\nu_\mu) \geq 6.0 \cdot 10^{24}$  y, and  $\tau(nn \rightarrow 2\nu_e) \geq 1.2 \cdot 10^{25}$  y [178].

6. Search for bremsstrahlung — quanta emitted due to the sudden disappearance of the neutron magnetic moment, suggested by Glicenstein. The mode-dependent limits have been obtained for the neutron lifetime  $\tau(n \rightarrow 3\nu_i) \geq 2.3 \cdot 10^{27}$  y, and  $\tau(n \rightarrow 5\nu_i) \geq 1.7 \cdot 10^{27}$  y, using the Kamiokande data on the  $\gamma$ -quanta flux with the energies higher than 100 MeV [179].

7. Study of the radioactive decay of the daughter nuclei, created as a result of the nucleon or dinucleon decays of the mother nuclei. This method was first exploited by the DAMA group with a liquid Xe detector [180]. The limit obtained for the lifetime of the  $^{129}\text{Xe}$  nucleus with respect to the decay  $nn \rightarrow 2\nu$ , is  $\tau \geq 1.2 \cdot 10^{25}$  y. This method, as well as the geochemical one, does not depend on the decay mode.

### 5.1. Search for Nucleon Decays with the Borexino Counting Test Facility.

The CTF-II detector has been used for the search of the nucleon decay in the

nuclei of carbon and oxygen [154]. If the daughter nuclei are radioactive, their decays can be detected.

Eight unstable nuclei are formed in the nucleon and dinucleon decays of two carbon isotopes  $^{12}\text{C}$  and  $^{13}\text{C}$ , and  $^{16}\text{O}$ ; half of them being  $\beta^-$  emitters; and

**Table 8. The daughter nuclei for the decays  $n \rightarrow 3\nu$ ,  $p \rightarrow 3\nu$ ,  $nn \rightarrow 2\nu$ ,  $pp \rightarrow 2\nu$  and  $np \rightarrow 2\nu$  in the stable isotopes of carbon and oxygen**

			$nn \rightarrow 2\nu$	$n \rightarrow 3\nu$	$N(A, Z)$
				$np \rightarrow 2\nu$	$p \rightarrow 3\nu$
					$pp \rightarrow 2\nu$
$Z = 8$			$^{14}\text{O} (\beta^+)$	$^{15}\text{O} (\beta^+)$	$^{16}\text{O} (\text{stable})$
$Z = 7$			$^{13}\text{N} (\beta^+)$	$^{14}\text{N} (\text{stable})$	$^{15}\text{N} (\text{stable})$
$Z = 6$	$^{10}\text{C} (\beta^+)$	$^{11}\text{C} (\beta^+)$	$^{12}\text{C} (\text{stable})$	$^{13}\text{C} (\text{stable})$	$^{14}\text{C} (\beta^-)$
$Z = 5$	$^9\text{B} (\beta^+)$	$^{10}\text{B} (\text{stable})$	$^{11}\text{B} (\text{stable})$	$^{12}\text{B} (\beta^-)$	
$Z = 4$	$^8\text{Be} (\text{stable})$	$^9\text{Be} (\text{stable})$	$^{10}\text{Be} (\beta^-)$	$^{11}\text{Be} (\beta^-)$	
	$N = 4$	$N = 5$	$N = 6$	$N = 7$	$N = 8$

the other half  $\beta^+$ , emitters (Table 8). The main characteristics of the daughter nuclei decay are shown in Table 9. The  $\beta^+$  decays of the  $^{11}\text{C}$  and  $^{10}\text{C}$  daughter nuclei can be registered in the case of the nucleon decay in  $^{12}\text{C}$ . The isotope  $^{10}\text{Be}$  has too big lifetime to be registered,  $T_{1/2} = 1.6 \cdot 10^6$  y, and can be removed at the stage of the scintillator purification. Despite the low abundance of the  $^{13}\text{C}$  isotope, just 1.1%, the decays  $p \rightarrow 3\nu$  and  $pn \rightarrow 2\nu$  in it result in the formation of the  $\beta^-$ -radioactive nuclei  $^{12}\text{B}$  and  $^{11}\text{Be}$  with an end-point energy of more than 10 MeV, which can be easily detected. Moreover, the lifetime of  $^{12}\text{B}$  is only 30 ms, which makes possible the selection of the delayed coincidences. The nucleon decay in the stable isotope  $^{16}\text{O}$  of the water shielding results in 3 radioactive daughter nuclei; but only the decays accompanied by the  $\gamma$  emission can be effectively detected, all other radiation is absorbed in the shielding. The  $^{14}\text{C}$  nucleus is  $\beta^-$ -decaying into the ground state, as well as the  $^{15}\text{O}$  nucleus ( $\beta^+$  decay). The latter can be in principle registered by the annihilation quanta. The best candidate is the  $^{14}\text{O}$  nucleus, which decays into the excited level of  $^{14}\text{N}$  with an almost 100% branching ratio, releasing in the de-excitation process a  $\gamma$ -quantum of 2.3 MeV energy and two annihilation quanta. In this way, 5 candidate daughter nuclei were selected for the search for the  $N$  and  $NN$  decays with the CTF detector.

After the nucleon disappearance, the daughter nucleus can be left in the excited state. If the excitation energy is higher than the minimal binding energy of the nucleons in the daughter nucleus, de-excitation with the emission of protons,

neutrons and  $\gamma$  particles instead of  $\gamma$  quanta is possible. These processes do not result in the listed nuclei and should be excluded from consideration. Appearance of the prompt  $\gamma$  quanta was not considered in the data analysis for two reasons: because of the big lifetimes of the daughter nuclei (excluding  $^{12}\text{B}$ ), and also

**Table 9. Candidate couples of parent-daughter nuclei: the initial isotope abundance, decay with  $\Delta B = 1, 2$ ; and characteristics of the daughter nuclei**

Parent nucleus, abundance	Decay	Daughter nucleus	$T_{1/2}$	The scheme of the decay
$^{12}_6\text{C}$ (98.9%)	$n$	$^{11}_6\text{C}$	20.4 m	$\beta^+$ (99.8%), $Q = 1.98$ MeV
	$p$	$^{11}_5\text{B}$	Stable	
	$nn$	$^{10}_6\text{C}$	19.2 s	$\beta^+$ , $Q = 3.65$ MeV
	$np$	$^{10}_5\text{B}$	Stable	
	$pp$	$^{10}_4\text{Be}$	$1.6 \cdot 10^6$ y	$\beta^-$ , $Q = 0.56$ MeV
$^{13}_6\text{C}$ (1.07%)	$n$	$^{12}_6\text{C}$	Stable	
	$p$	$^{12}_5\text{B}$	20.4 ms	$\beta^-$ , $Q = 13.37$ MeV
	$nn$	$^{11}_6\text{C}$	20.4 m	$\beta^+$ (99.8%), $Q = 1.98$ MeV
	$np$	$^{11}_5\text{B}$	Stable	
	$pp$	$^{11}_4\text{Be}$	13.8 s	$\beta^-$ , $Q = 11.51$ MeV
$^{16}_8\text{O}$ (99.8%)	$n$	$^{15}_8\text{O}$	122 s	$\beta^+$ (99.9%), $Q = 2.75$ MeV
	$p$	$^{15}_7\text{N}$	Stable	
	$nn$	$^{14}_8\text{C}$	70.6 s	$\beta^+$ , $Q = 5.15$ MeV
	$np$	$^{14}_7\text{B}$	Stable	
	$pp$	$^{14}_6\text{C}$	5730 y	$\beta^-$ , $Q = 0.156$ MeV

due to the uncertainties in the number of the emitted quanta, their energy, and suppression of these events by the muon veto. Thus, it is necessary to define the number of the nucleons and nucleon pairs in the mother nucleus for which the daughter nucleus will emit only  $\gamma$  quanta. For this purpose the following method can be used [171, 180]. After the decay of the nucleon (for simplicity, let us assume that it is a neutron) in the mother nucleus  $N(A, Z)$  with binding energy  $E_n^b(A, Z)$ , the daughter nucleus is left in the excited state with the energy  $E_{\text{exc}} = E_n^b(A, Z) - S_n(A, Z)$ , where  $S_n(A, Z)$  is the binding energy of the last nucleon (neutron in our case) in the  $N(A, Z)$  nucleus. The excitation energy should be lower than the minimal binding energy of the last proton, neutron or  $\alpha$  particle in the daughter nucleus  $S_{N_{\text{min}}}(A-1, Z)$ ; this condition will guarantee de-excitation by  $\gamma$  quanta. In this way, the condition of nondestruction of the daughter nucleus

is:  $E_n^b(A, Z) < S_n(A, Z) + S_{N_{\min}}(A - 1, Z)$ . The same conditions can be written for the decay of the proton,  $np$  and  $pp$  pairs. For example, for the case of a two neutron decay the condition for the binding energies of the decaying neutron is:  $E_{n1}^b(A, Z) + E_{n2}^b(A, Z) < S_{2n}(A, Z) + S_{N_{\min}}(A - 2, Z)$ . The values of the upper limits on the binding energy of the decaying nucleons and nucleon pairs are shown in Table 10. The values of the nucleon binding energies  $S_N$ ,  $S_{NN}$  are from [152].

**Table 10. Separation energies  $S_n$ ,  $S_p$ , and  $S_\alpha$  for the parent and daughter nuclei. Upper limits on the nucleon binding energies ensuring de-excitation of the daughter nucleus by  $\gamma$  quanta**

Decay	Transition	$S_{n,p}, S_{nn,pp}$ of the parent nucleus	$S_n$ of the daughter nucleus	$S_p$ of the daughter nucleus	$S_\alpha$ of the daughter nucleus	Limit on $E_N^b$ , $E_{N1}^b + E_{N2}^b$
$p$	$^{13}_6\text{C} \rightarrow ^{12}_5\text{B}$	17.5	3.4	14.1	10.0	20.9
$n$	$^{12}_6\text{C} \rightarrow ^{11}_6\text{C}$	18.7	13.1	8.7	7.5	26.2
$nn$	$^{12}_6\text{C} \rightarrow ^{10}_6\text{C}$	31.8	21.3	4.0	5.1	35.8
$nn$	$^{16}_8\text{O} \rightarrow ^{14}_8\text{O}$	28.9	23.2	4.6	10.1	33.5
$pp$	$^{13}_6\text{C} \rightarrow ^{11}_4\text{Be}$	31.6	0.5	11.5	8.7	32.1

Comparing the obtained limits on the binding energies with the shell energies  $1S_{1/2}$  and  $1P_{3/2}$  for  $^{12}\text{C}$  nucleus (Table 10), one can conclude that the decays  $n \rightarrow 3\nu$  and  $nn \rightarrow 2\nu$  for the nucleons on  $1P_{3/2}$  shell are accompanied only by  $\gamma$  quanta. The same scenario is realized for the decays  $p \rightarrow 3\nu$  and  $pp \rightarrow 2\nu$  in  $^{13}\text{C}$  nucleus. Only a pair of neutrons on  $1P_{1/2}$  shell satisfies the condition of nondestruction of the daughter nucleus for the decay  $nn \rightarrow 2\nu$  in the  $^{16}\text{O}$  nucleus.

The expected response functions of the CTF detector and related efficiencies for the decay of the unstable daughter nuclei  $^{10}\text{C}$ ,  $^{11}\text{C}$ ,  $^{14}\text{O}$ ,  $^{12}\text{B}$ , and  $^{11}\text{Be}$  were simulated with the EGS4 package. The number of the initial electrons and  $\gamma$  quanta emitted in the decay of the nucleus and their energies were generated according to the decay schemes [181]. The events were supposed to be uniformly distributed in the whole volume of the liquid scintillator and in the 1 m thick water layer close to the LS. The energy and spatial resolution of the detector, ionization quenching factors for the electrons and gammas, muon veto and triggering efficiency were taken into account in the simulations. The calculated responses for the decays of  $^{10}\text{C}$ ,  $^{11}\text{C}$ , and  $^{14}\text{O}$  in the liquid scintillator are shown in Fig. 9 in comparison with the observed background spectrum.

The experimental data give no strong evidence of the expected  $N$  and  $NN$  decay response functions, thus allowing bounds only to be set on the processes

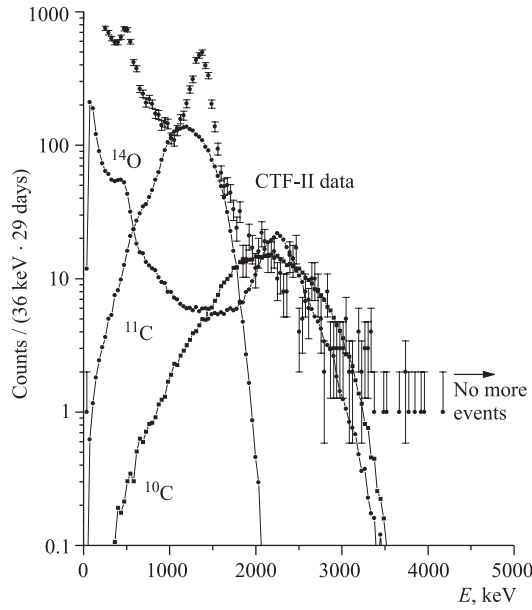


Fig. 9. Energy distribution of the CTF-II installation collected during 29 days with all the cuts. The expected response functions of the detector are also shown for  $^{11}\text{C}$  ( $3.4 \cdot 10^3$  decays in the liquid scintillator; the corresponding mean lifetime for the  $nn$  decay is  $\tau_{nn} = 1.8 \cdot 10^{25}$  y),  $^{10}\text{C}$  ( $6.8 \cdot 10^2$  decays;  $\tau_{nn} = 4.4 \times 10^{25}$  y), and  $^{14}\text{O}$  ( $1.4 \cdot 10^4$  decays in a 1 m thick water layer around the sphere with the liquid scintillator;  $\tau_{nn} = 5.7 \cdot 10^{24}$  y)

being searched for. In order to extract the limits on the relevant mean lifetimes, in the study it was conservatively assumed that *all* events in the CTF-II experimental spectrum in the corresponding energy range  $\Delta E$  are due to nucleon decays.

The mean lifetime limit was estimated using the formula

$$\tau_{\text{lim}} = \varepsilon_{\Delta E} N_{\text{nucl}} N_{\text{obj}} t / S_{\text{lim}} = N_{\text{nucl}} N_{\text{obj}} t / D_{\text{lim}}, \quad (21)$$

where  $\varepsilon_{\Delta E}$  is the detection efficiency in the  $\Delta E$  energy window calculated in the full simulation of the relevant process, taking into account the radial cut efficiency  $\varepsilon_R$ , and probability of identification by the muon veto  $\eta$ ;  $N_{\text{nucl}}$  is the number of parent nuclei;  $N_{\text{obj}}$  is the number of objects ( $n$ ,  $p$  or  $NN$  pairs) inside the parent nucleus whose decay will give a specific daughter nucleus;  $t$  is the time of measurements;  $S_{\text{lim}}$  is the number of events (in the  $\Delta E$  window) due to a particular effect which can be excluded with a given confidence level on the basis of experimental data; and  $D_{\text{lim}} = S_{\text{lim}} / \varepsilon_{\Delta E}$  is the corresponding number of decays in the liquid scintillator/water.

For the  $nn$  decay, there are four neutrons at the outermost  $1P_{3/2}$  level of  $^{12}\text{C}$  which gives the number of  $nn$  pairs  $N_{\text{obj}} = 2$ . The disappearance of the  $nn$  pair from this level will result in a  $^{10}\text{C}$  nucleus in the ground state. For the  $^{16}\text{O}$  nucleus only one  $nn$  pair has been taken into account in the outermost  $1P_{1/2}$  orbit (the  $nn$  decay in the deeper levels will result in the  $^{16}\text{O}$  nucleus being too excited).

For the  $n$  decay in  $^{12}\text{C}$  a similar approach has been used, comparing the simulated response function for the  $^{11}\text{C}$  decay with the experimental spectrum in the energy region 1.0–1.1 MeV (Fig. 9).

As for the  $p$  and  $pp$  decays into the invisible channels, the  $p$  disappearance in  $^{13}\text{C}$  will result in  $^{12}\text{B}$  nuclei,  $\beta^-$ -decaying with a high energy release,  $Q = 13.370$  MeV. The  $pp$  decays in  $^{13}\text{C}$  will produce  $^{11}\text{Be}$  nuclei, also  $\beta^-$ -decaying with  $Q = 11.508$  MeV (with a probability of a decay to the ground state of 57%). The fact that no candidate scintillation events were observed in the CTF-II spectrum with the energies higher than 4.5 MeV (Fig. 8) allows one to estimate  $\tau_{\text{lim}}$  for the  $p$  and  $pp$  instabilities. The suppression of high-energy tails in the  $\beta$  decays of  $^{12}\text{B}$  and  $^{11}\text{Be}$  has been taken into account using the probability  $\eta(E)$  for identification of an event with the energy  $E$  in the LS by the muon veto.

Table 11. Mean lifetime limits,  $\tau_{\text{lim}}$  (at 90% CL) for the  $N$  and  $NN$  decays in the CTF-II

	Decay	$N_{\text{nucl}}$	$N_{\text{obj}}$	$D_{\text{lim}}$	$\tau_{\text{lim}}, \text{y}$	Previous
$p$	$^{13}_6\text{C} \rightarrow ^{12}_5\text{B}$	$2.1 \cdot 10^{27}$	4	6.2	$1.1 \cdot 10^{26}$	$3.5 \cdot 10^{28}$ [170]
$n$	$^{12}_6\text{C} \rightarrow ^{11}_6\text{C}$	$1.9 \cdot 10^{29}$	4	$3.4 \cdot 10^3$	$1.8 \cdot 10^{25}$	$2.3 \cdot 10^{27}$ [179]
$nn$	$^{12}_6\text{C} \rightarrow ^{10}_6\text{C}$	$1.9 \cdot 10^{29}$	2	$6.8 \cdot 10^2$	$4.4 \cdot 10^{25}$	$1.2 \cdot 10^{25}$ [178]
	$^{16}_8\text{O} \rightarrow ^{14}_8\text{O}$	$9.8 \cdot 10^{29}$	1	$1.4 \cdot 10^4$	$5.7 \cdot 10^{24}$	—
$pp$	$^{13}_6\text{C} \rightarrow ^{11}_4\text{Be}$	$2.1 \cdot 10^{27}$	2	6.7	$5.0 \cdot 10^{25}$	$5.5 \cdot 10^{23}$ [180]

Note.  $N_{\text{nucl}}$  is the number of parent nuclei;  $N_{\text{obj}}$  is the number of objects ( $n$ ,  $p$ , and  $NN$  pairs) per parent nucleus;  $D_{\text{lim}}$  is the excluded number of decay events.

All the mean lifetime limits obtained, together with the numbers of parent nuclei,  $N_{\text{obj}}$ , and the numbers of decay events are summarized in Table 11. One can see that the established limits for  $nn$  and  $pp$  decays are the best up-to-date limits set by any method, including radiochemical and geochemical experiments.

## 6. EXPERIMENTAL LIMITS ON THE HEAVY NEUTRINO MIXING IN THE $^8\text{B}$ DECAY

If neutrinos have mass, then the heavier one can decay to a lighter one [87, 182]. The simplest detectable decay modes in the framework of an extended Standard Model (SM) are the radiative decay  $\nu_H \rightarrow \nu_L + \gamma$  and decay into an electron, positron and a light neutrino:

$$\nu_H \rightarrow \nu_L + e^+ + e^-. \quad (22)$$

The  $e^+e^-$  decay mode, which becomes possible if  $m_{\nu_H} \geq 2m_e$ , results from a  $W$  exchange diagram, as shown in Fig. 10.

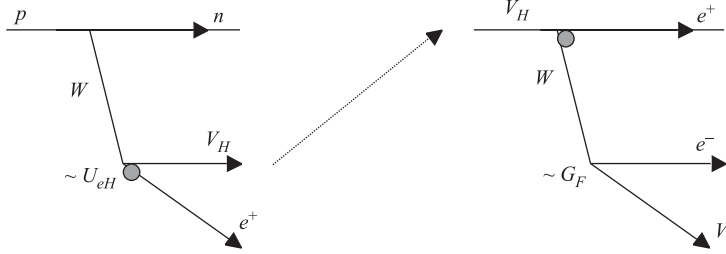


Fig. 10. Feynman graphs describing the appearance ( ${}^8\text{B} \rightarrow {}^8\text{Be} + e^+ + \nu_H$ ) and decay ( $\nu_H \rightarrow \nu_L + e^+ + e^-$ ) of a heavy neutrino

After the discovery of the atmospheric, solar and reactor neutrino oscillations, the heavy neutrino cannot be associated with one of the three mass eigenstates forming three known neutrino flavors. Moreover, this fourth neutrino has to be coupled in the  $(e - W)$  vertex with the  $U_{eH}$  and  $G_F$  constants but it cannot be coupled (or coupled very weakly) to the  $Z$  boson. Many extensions of the SM predict the existence of a sterile neutrino: a singlet fermion can be a mirror neutrino, goldstino in SUSY, modulino of the superstring theories, or a bulk fermion related to the existence of extra dimensions [183]. In general, the sterile neutrino may have an arbitrary mass and can mix with all the three active neutrinos.

The decay rate for this mode in the centre-of-mass system of the decaying neutrino is [87, 182]:

$$\Gamma_{\text{cm}} \cong \frac{G_F^2}{192\pi^3} m_{\nu_H}^5 |U_{eH}|^2 |U_{eL}|^2 h \left[ \frac{m_e^2}{m_{\nu_H}^2} \right], \quad (23)$$

where  $U_{eH}$  is the mixing parameter of the heavy neutrino to the electron,  $G_F^2/192\pi^3 = 3.5 \cdot 10^{-5} \text{ MeV}^{-5} \cdot \text{s}^{-1}$ ;  $h[m_e^2/m_{\nu_H}^2]$  is the phase-space factor calculated in [87]; the mixing parameter of the light neutrino  $U_{eL}$  satisfies the condition  $|U_{eL}|^2 \simeq 1$ . In the SM the probability of the  $e^+e^-$  mode is much higher than for radiative decay: e.g., for  $m_{\nu_H} = 5 \text{ MeV}$  (and  $|U_{eH}|^2 \sim 1$ ) one obtains  $\tau(\nu_H \rightarrow \nu_L e^+ e^-) \approx 10 \text{ s}$  against  $\tau(\nu_H \rightarrow \nu_L \gamma) \sim 10^{10} \text{ s}$ .

The possible decay of massive antineutrinos from a reactor  $\nu_H \rightarrow \nu_L + e^+ + e^-$  was studied in [184–187]; the latter gives the strongest restrictions on the mixing parameter ( $|U_{eH}|^2 < (0.3 - 5) \cdot 10^{-3}$  in the mass region  $m_{\nu_H} \sim (1.1 - 9.5) \text{ MeV}$ ). Accelerator experiments performed in a beam of neutrinos from the  $\pi$  and  $K$  decays constrain the coupling of still heavier neutrinos (see [18] and refs. therein). A heavy neutrino with a mass up to 15 MeV can be produced in

the Sun in the reaction  ${}^8\text{B} \rightarrow {}^8\text{Be} + e^+ + \nu$ , then it can decay in flight. The upper limit  $|U_{eH}|^2 \sim 10^{-5}$  was obtained by considering data on the positron flux in the interplanetary space [188].

More restrictive bounds were obtained from the SN1987A data [189–192]. On the other hand, the Big Bang nucleosynthesis requires a fast decay branch ([189–192] and refs. therein). This fast mode could be realized by the decay of a heavy particle into a Goldstone boson and a light neutrino. Obviously, this decay mode should be slower than  $\simeq 500$  s, which is the time needed for the particle to reach the detector.

The bounds on the parameters  $|U_{eH}|^2$  and  $m_\nu$  were obtained from the CTF-II spectrum, comparing it with the energy spectrum expected for the  $\nu_H$ -decay [193]. To calculate the latter, one has to know the flux of heavy neutrinos through the detector  $\Phi(E_\nu)$ , kinetic energy of the created  $e^+e^-$  pairs, and the response function of CTF-II to two annihilation quanta.

The emission of a heavy neutrino, coupled to an electron, in the  $\beta^+$  decay of  ${}^8\text{B}$  is suppressed by the mixing parameter  $|U_{eH}|^2$  and a phase-space factor:

$$\Phi_{m_\nu}(E_\nu) = |U_{eH}|^2 \sqrt{1 - \left(\frac{m_{\nu H}}{E_\nu}\right)^2} \Phi_{sB}(E_\nu), \quad (24)$$

where  $E_\nu$  is the total energy of the heavy neutrino ( $\Phi_{m_\nu}(E_\nu) = 0$  for  $E_\nu < m_\nu$ ). The neutrino spectrum from the  ${}^8\text{B}$  decay  $\Phi_{sB}(E_\nu)$  given in [79] has been used in the calculation.

The heavy neutrino emitted in the Sun can decay in its flight to the Earth. The energy spectrum of the neutrinos reaching the detector is given by

$$\Phi(E_\nu) = \exp(-\tau_f/\tau_{\text{cm}}) \Phi_{m_\nu}(E_\nu),$$

where  $1/\tau_{\text{cm}} = \Gamma_{\text{cm}}$  according to (23).  $\tau_f$  is the time of flight in c.m.s.

$$\tau_f = \frac{m_{\nu H}}{E_\nu} \frac{L}{\beta c}. \quad (25)$$

Here  $L = 1.5 \cdot 10^{13}$  cm is the average distance between Sun and Earth and  $\beta = \sqrt{1 - (m_\nu/E_\nu)^2}$ .

The double differential distribution for the energy  $\epsilon$  and emission angle  $\theta$  of the light neutrino  $\nu_L$  for the c.m.s. was obtained in [194].

The experiment is not as sensitive for the low  $|U_{eH}|^2$  (due to the low probability of the  $\nu_H$  decay) as for the high values of  $|U_{eH}|^2$  because in this case  $\nu_H$  decays during its flight from the Sun. The maximum  $S_{\text{int}}(|U_{eH}|^2)$  for the fixed  $m_\nu$  and  $E_\nu$  corresponds to  $|U_{eH}|^2 = 2(|U_{eH}|^2 \tau_{\text{cm}})/\tau_f$ , where  $\tau_{\text{cm}} = 1/\Gamma_{\text{cm}}$  and  $\tau_f$  are defined by (23) and (25). The region of restricted values of the parameters

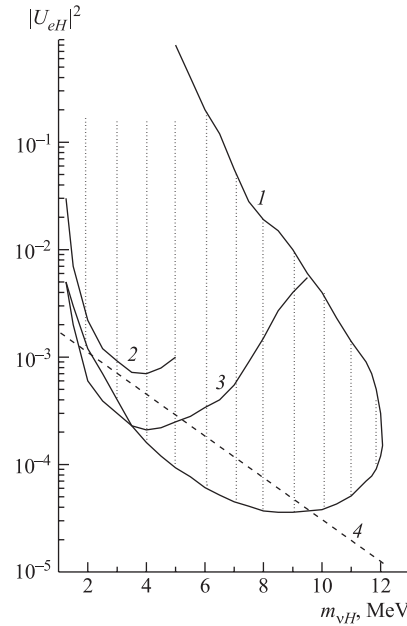


Fig. 11. Limits on the mixing parameter  $|U_{eH}|^2$  as a function of neutrino mass  $m_\nu$  (90% CL). 1 — the present work excludes the values of  $|U_{eH}|^2$  and  $m_\nu$  inside the dotted region; 2, 3 — upper limits from the reactor experiments on the search for the  $\nu_H \rightarrow \nu_L + e^+ + e^-$  decay [34, 187]; 4 — upper limits from the  $\pi \rightarrow e + \nu$  decay [195]

$|U_{eH}|^2$  and  $m_\nu$  are shown in Fig. 11 in comparison with the results of the reactor experiments [34, 184–187] and the search for massive neutrinos in the decay  $\pi^+ \rightarrow e^+ \nu_e$  in accelerators [195]. For the neutrino mass region 4–10 MeV the obtained limits on the mixing parameter are stronger than those obtained in the previous experiments using nuclear reactors and accelerators.

## CONCLUSIONS

Presented discussion of the selected topics in the field of the experimental nonaccelerating physics demonstrates an extraordinary sensitivity of the Borexino prototype to the rare processes. Despite of the comparatively small detectors's volume the achieved background level permitted to obtain a number of new physical results:

- The limits on the electromagnetic properties of low-energy neutrinos. A new upper limit on the neutrino magnetic moment from the  $pp$ - and  ${}^7\text{Be}$ -solar

neutrinos is  $\mu_\nu \leq 5.5 \cdot 10^{-10} \mu_B$  (90% CL) in the assumption of SSM neutrino fluxes. This value is only 3 times weaker than the ones obtained using reactor neutrinos and  $^8\text{B}$ -solar neutrinos.

- The lower limit on the mean lifetime of the  $pp$  and  $^7\text{Be}$  neutrino relative radiative decay is obtained:  $\tau_{\text{cm}}(\nu_H \rightarrow \nu_L + \gamma)/m_\nu \geq 4.2 \cdot 10^3 \text{ s} \cdot \text{eV}^{-1}$  ( $\alpha = 0$ ). It is more than one order of magnitude stronger than that obtained in the previous experiments using nuclear reactors and accelerators.

- A new lower limit on the mean lifetime for the decay  $e \rightarrow \gamma + \nu$  is established:  $\tau \geq 4.6 \cdot 10^{26} \text{ y}$  (90% CL).

- New limits on the non-Paulian transitions of nucleons from the  $P$  shell to the  $1S_{1/2}$  shell in  $^{12}\text{C}$  and  $^{16}\text{O}$  with emission of  $\gamma, n, p, \alpha$ , and  $\beta^\pm$  particles are obtained.

- New limits on the  $N$  and  $NN$  decays into the invisible channels (disappearance, decays to neutrinos, majorons, etc.) are set. The established limits for the  $nn$  and  $pp$  decays ( $\tau(nn \rightarrow \text{inv}) > 4.9 \cdot 10^{25} \text{ y}$ ,  $\tau(pp \rightarrow \text{inv}) > 5.0 \cdot 10^{25} \text{ y}$  with 90% CL) are the best up-to-date limits set by any method, including radiochemical and geochemical experiments.

- New limits on the mixing parameter  $|U_{eH}|^2$  of a massive neutrino in the mass range 1.1–12 MeV are set. These limits are more than one order of magnitude stronger than those obtained in the previous experiments using nuclear reactors.

These results show the sensitivity level of the modern low-background low-threshold liquid scintillator detectors. One can expect significant improvement of the discussed limits with a larger detectors, such as the full-scale 300 t Borexino detector or the upgraded version of the 1000 t KamLAND detector with a lower threshold.

**Acknowledgements.** This work was performed with the support of the INFN Milano section in accordance with the scientific agreement on Borexino between the INFN and JINR (Dubna), and between JINR and the PNPI (Gatchina). We would like to thank personally Prof. G. Bellini and Dr. G. Ranucci. Many thanks to all our colleagues from the Borexino collaboration for the pleasure of working together. The authors appreciate the help of E. Petrus in preparation of the manuscript.

#### REFERENCES

1. *Glashow S. L.* // Nucl. Phys. 1961. V. 22. P. 579;  
*Weinberg S.* // Phys. Rev. Lett. 1967. V. 19. P. 1264;  
*Salam A.* Elementary Particle Theory. Stockholm, 1969. P. 367;  
 for review see *Okun L. B.* Leptons and Quarks. M.: Nauka, 1990;  
*Langacker P., Ertler J.* Review of Particle Properties // Phys. Rev. D. 1994. V. 50. P. 1304.
2. *Pauli W.* // Z. Phys. 1925. V. 31. P. 765.

3. <http://www-sk.icrr.u-tokyo.ac.jp/doc/sk>
4. <http://www.awa.tohoku.ac.jp/KamLAND/>
5. Eguchi K. *et al.* // Phys. Rev. Lett. 2003. V. 90. P. 021802.
6. Suzuki A. // Nucl. Phys. B (Proc. Suppl.). 1999. V. 77. P. 171.
7. <http://www.sno.phy.queensu.ca/>
8. Alimonti G. *et al.* (Borexino Collab.) // Astropart. Phys. 2002. V. 16. P. 205.
9. Alimonti G. *et al.* (Borexino Collab.) // Nucl. Instr. Meth. A. 1998. V. 406. P. 411; Astropart. Phys. 1998. V. 8. P. 141; Phys. Lett. B. 1998. V. 422. P. 349.
10. Alimonti G. *et al.* (Borexino Collab.) // Nucl. Instr. Meth. A. 2000. V. 440. P. 360.
11. Birks J. B. // Proc. Phys. Soc. A. 1951. V. 64. P. 874.
12. Smirnov O. Ju. // Instr. Exp. Tech. 2003. V. 46. P. 327.
13. <http://www.lngs.infn.it/lngs/htexts/dama/>
14. Kayser B. // Phys. Rev. D. 1982. V. 26. P. 1662.
15. Marinelli M., Morpurgo G. // Phys. Lett. B. 1984. V. 137. P. 439.
16. Baumann J. *et al.* // Phys. Rev. D. 1988. V. 37. P. 3107.
17. Raffelt G. G. // Phys. Rep. 1999. V. 320. P. 319.
18. Groom D. E. *et al.* (Particle Data Group) // Eur. Phys. J. C. 2000. V. 15. P. 1; Hagiwara K. *et al.* // Phys. Rev. D. 2002. V. 66. P. 010001.
19. Marciano W. J., Sirlin A. // Phys. Rev. D. 1980. V. 22. P. 2695.
20. Vogel P., Engel J. // Phys. Rev. D. 1989. V. 39. P. 3378.
21. Auerbach L. B. *et al.* (LSND Collab.) // Phys. Rev. D. 2001. V. 63. P. 112001.
22. Allen R. C. *et al.* // Phys. Rev. D. 1993. V. 47. P. 11.
23. Vilain P. *et al.* // Phys. Lett. B. 1995. V. 345. P. 115.
24. Ahrens L. A. *et al.* // Phys. Rev. D. 1990. V. 41. P. 3297.
25. Jshipura A., Mohanty S. hep-ph/0108018; hep-ph/0204305.
26. Ianni A. // Phys. Lett. B. 2002. V. 540. P. 20.
27. Weinheimer Ch. // Nucl. Phys. B (Proc. Suppl.). 2003. V. 118.
28. Lobashev V. M. *et al.* // Phys. Lett. B. 1999. V. 460. P. 227.
29. Cowan C. L., Reines F. // Phys. Rev. 1957. V. 107. P. 528.
30. Kyuldiev A. V. // Nucl. Phys. B. 1984. V. 234. P. 387.
31. Vogel H., Engel J. // Phys. Rev. D. 1989. V. 39. P. 3378.
32. Derbin A. V. // Phys. At. Nucl. 1994. V. 57. P. 236.
33. Vidyakin G. S. *et al.* // JETP Lett. 1992. V. 55. P. 212.
34. Derbin A. V. *et al.* // JETP Lett. 1993. V. 57. P. 755.
35. Derbin A. V. // Part. Nucl. 2001. V. 32. P. 734.
36. Li H. B. *et al.* // Phys. Rev. Lett. 2003. V. 90. P. 131802.
37. Daraktchieva Z. *et al.* // Phys. Lett. B. 2003. V. 564. P. 190.
38. Krakauer D. A. *et al.* // Phys. Lett. B. 1990. V. 252. P. 177.

39. Abe K. *et al.* // Phys. Rev. Lett. 1987. V. 58. P. 636.
40. Schwienhorst R. *et al.* (*DONUT Collab.*) // Phys. Lett. B. 2001. V. 513. P. 23.
41. Pulido J., Mourao A. M. // Phys. Rev. D. 1998. V. 57. P. 1794.
42. Beacom J. F., Vogel P. // Phys. Rev. Lett. 1999. V. 83. P. 5222.
43. Liu D. W. *et al.* (*Super-Kamiokande Collab.*). hep-ex/0402015.
44. Akhmedov E. Kh. // Yad. Fiz. 1988. V. 48. P. 599; Phys. Lett. B. 1988. V. 213. P. 64.
45. Lim G. S., Marciano W. J. // Phys. Rev. D. 1988. V. 37. P. 1368.
46. Akhmedov E. Kh., Pulido J. // 2000. V. 485. P. 178; Phys. Lett. B. 2002. V. 529. P. 193.
47. Bahcall J. N., Pinsonneault M. H. // Rev. Mod. Phys. 1992. V. 64. P. 885.
48. Lande K. // Proc. of Neutrino-96. World Scientific, 1996. P. 25.
49. Abdurashitov J. N. *et al.* (*SAGE Collab.*) // ZhETF. 2002. V. 122. P. 1.
50. Kirsten T. (*GNO Collab.*) // Nucl. Phys. B (Proc. Suppl.). 2003. V. 118. P. 230.
51. Suzuki K. Y. (*Kamiokande Collab.*) // Proc. of Neutrino-96. World Scientific, 1996. P. 73.
52. Fukuda S. *et al.* (*SuperKamiokande Collab.*) // Phys. Lett. B. 2002. V. 539. P. 179.
53. Ahmad Q. R. *et al.* (*SNO Collab.*) // Phys. Rev. Lett. 2001. V. 89. P. 011301.
54. Cisneros A. // Astrophys. Space Sci. 1971. V. 10. P. 87.
55. Fujikawa K., Shrock R. // Phys. Rev. Lett. 1980. V. 45. P. 963.
56. Bazilevskaya G. A. *et al.* // JETP Lett. 1982. V. 35. P. 273.
57. Gavrín V. N. *et al.* // *Ibid.* P. 491.
58. Bahcall J. N. Neutrino Astrophysics. Cambridge: Cambridge Univ. Press, 1989.
59. Voloshin M. B., Vysotsky M. I. // PAN. 1986. V. 44. P. 845.
60. Okun L. B. // *Ibid.* P. 847.
61. Voloshin M. B., Vysotsky M. I., Okun L. B. // JETP. 1986. V. 44. P. 677.
62. Oakley D. S. *et al.* // Astrophys. J. 1994. V. 437. P. L63.
63. Walter G. // Phys. Rev. Lett. 1997. V. 79. P. 4522.
64. Sturrock P. A., Walter G., Wheatland M. S. // Astrophys. J. 1998. V. 507. P. 978.
65. Cadwell D. O., Sturrock P. A. hep-ph/0309191; astro-ph/0307353; hep-ph/0304106.
66. Miranda O. G. *et al.* // Phys. Lett. B. 2001. V. 521. P. 299.
67. Gago A. M. *et al.* hep-ph/0112060.
68. Barraco J. *et al.* hep-ph/0207326.
69. Schechter J., Valle J. W. // Phys. Rev. D. 1981. V. 24. P. 1883.
70. Schechter J., Valle J. W. // Phys. Rev. D. 1982. V. 25. P. 774.
71. Gelmini G. B., Valle J. W. // Phys. Lett. B. 1984. V. 142. P. 181.
72. Gonzalez-Garcia M. C., Valle J. W. // Phys. Lett. B. 1989. V. 216. P. 360.
73. Beacom J. F., Bell N. F. // Phys. Rev. D. 2002. V. 65. P. 113009.
74. Cando Y. *et al.* (*SuperKamiokande Collab.*) // Phys. Rev. Lett. 2003. V. 90. P. 171302.
75. Eguchi K. *et al.* (*KamLAND Collab.*) // Phys. Rev. Lett. 2004. V. 92. P. 071301.
76. Miranda O. G. hep-ph/0311014. 2003.

77. Grimus W. *et al.* hep-ph/0208132.
78. Back H. O. *et al.* (Borexino Collab.) // Phys. Lett. B. 2003. V. 563. P. 35.
79. Bahcall J. N., Pinsonneault H., Basu S. // Astrophys. J. 2001. V. 555. P. 990.
80. Bahcall J. N. // Phys. Rev. C. 1997. V. 56. P. 3391.
81. Lee B. W., Shrock R. E. // Phys. Rev. D. 1997. V. 16. P. 1444.
82. Petcov S. T. // Yad. Fiz. 1977. V. 25. P. 641.
83. Sato E., Kobayashi M. // Prog. Theor. Phys. 1977. V. 58. P. 1775.
84. Beg M. A., Marciano W. J., Ruderman M. // Phys. Rev. D. 1978. V. 17. P. 1395.
85. de Rujula A., Glashow S. L. // Phys. Rev. Lett. 1980. V. 45. P. 942.
86. Pal P. B., Wolfenstein L. // Phys. Rev. D. 1982. V. 25. P. 766.
87. Shrock R. E. // Nucl. Phys. B. 1982. V. 296. P. 359.
88. Boem F., Vogel P. Physics of Massive Neutrinos. Cambridge: Cambridge University Press, 1992.
89. Reines F. *et al.* // Phys. Rev. Lett. 1974. V. 32. P. 180.
90. Vogel P. // Phys. Rev. D. 1984. V. 30. P. 1505.
91. Zacek G. *et al.* // Phys. Rev. D. 1986. V. 34. P. 2621.
92. Oberauer L., Von Feilitzsch F., Mossbauer R. L. // Phys. Lett. B. 1987. V. 198. P. 113.
93. Krakauer D. A. *et al.* // Phys. Rev. D. 1991. V. 44. P. 44.
94. Raffelt G. G. // Phys. Rev. D. 1985. V. 31. P. 3002.
95. Derbin A. V., Smirnov O. Ju. // JETP Lett. 2002. V. 76. P. 483.
96. Derbin A. V. *et al.* Preprint PNPI-2003, N2504. 2003.
97. Nelson W. R., Hirayama H., Rogers D. W. O. The EGS4 Code System. SLAC-265. 1985.
98. Oberauer L. *et al.* // Astropart. Phys. 1993. V. 1. P. 377.
99. Okun L. B., Zeldovich Ya. B. // Phys. Lett. B. 1978. V. 78. P. 597.
100. Voloshin M. B., Okun L. B. // JETP Lett. 1978. V. 28. P. 145.
101. Aharanov Y. *et al.* // Phys. Rev. D. 1995. V. 52. P. 3785.
102. Ignatiev A. Y., Kuzmin V. A., Shaposhnikov M. E. // Phys. Lett. B. 1979. V. 84. P. 315.
103. Dolgov A. D., Zeldovich Ya. B. // Rev. Mod. Phys. 1981. V. 53. P. 1.
104. Okun L. B. Leptons and Quarks. Amsterdam, 1982. P. 181.
105. Suzuki M. // Phys. Rev. D. 1988. V. 38. P. 1544.
106. Okun L. B. // Comments Nucl. Part. Phys. 1989. V. 19. P. 99.
107. Okun L. B. // Phys. Usp. 1989. V. 158. P. 293; (Sov. Phys. Usp. 1989. V. 32. P. 543).
108. Bahcall J. N. Neutrino Astrophysics. Cambridge, 1993. P. 360.
109. Ejiri H. *et al.* // Phys. Lett. B. 1992. V. 282. P. 281.
110. Feinberg G., Goldhaber M. // Proc. Nat. Acad. Sci. USA. 1959. V. 45. P. 1301.
111. Steinberg R. I. *et al.* // Phys. Rev. D. 1975. V. 12. P. 2582.
112. Moe M. K., Reines F. // Phys. Rev. 1965. V. 140. P. 992.
113. Kovalchuk E. L., Pomanski A. A., Smolnikov A. A. // JETP Lett. 1979. V. 29. P. 145.
114. Bellotti E. *et al.* // Phys. Lett. B. 1983. V. 124. P. 435.

115. Avignone F. T. III *et al.* // Phys. Rev. D. 1986. V. 34. P. 97.
116. Balysh A. *et al.* // Phys. Lett. B. 1993. V. 298. P. 278.
117. Aharanov Y. *et al.* // Phys. Lett. B. 1995. V. 353. P. 168.
118. Belli P. *et al.* // Astropart. Phys. 1996. V. 5. P. 217.
119. Belli P. *et al.* // Phys. Rev. D. 2000. V. 61. P. 117301.
120. Back H. O. *et al.* (Borexino Collab.) // Phys. Lett. B. 2002. V. 525. P. 29.
121. Belli P. *et al.* // Phys. Lett. B. 1999. V. 460. P. 236.
122. Rubakov V. A. // Phys. Usp. 2001. V. 44. P. 871.
123. Dubovsky S. L., Rubakov V. A., Tinyakov P. G. hep-ph/00007179.
124. Reusser D. *et al.* // Phys. Lett. B. 1991. V. 225. P. 143.
125. Ejiri H. *et al.* // Phys. Rev. C. 1991. V. 44. P. 502.
126. Holjevic S. *et al.* // Phys. Rev. C. 1987. V. 35. P. 341.
127. Norman E. B., Bahcall J. N., Goldhaber M. // Phys. Rev. D. 1996. V. 53. P. 4086.
128. Sunyar A. W., Goldhaber M. // Phys. Rev. 1960. V. 120. P. 871.
129. Norman E. B., Seamster A. G. // Phys. Rev. Lett. 1979. V. 43. P. 1226.
130. Barabanov I. R. *et al.* // JETP Lett. 1980. V. 32. P. 359.
131. Vaidya S. C. *et al.* // Phys. Rev. D. 1983. V. 27. P. 436.
132. Roy A. *et al.* // Phys. Rev. D. 1983. V. 28. P. 1770.
133. Klimenko A. A. *et al.* // Phys. Lett. B. 2002. V. 535. P. 77.
134. Belli P. *et al.* // Phys. Lett. B. 1999. V. 465. P. 315.
135. Belli P. *et al.* // Phys. Rev. C. 2000. V. 60. P. 065501.
136. Reines F., Sobel H. W. // Phys. Rev. Lett. 1974. V. 32. P. 954.
137. Logan B. A., Ljubičić A. // Phys. Rev. C. 1979. V. 20. P. 1957.
138. Amado R. D., Primakoff H. // Phys. Rev. C. 1980. V. 22. P. 1338.
139. Ignatiev A. Yu., Kuzmin V. A. // Sov. J. Nucl. Phys. 1987. V. 461. P. 786.
140. Greenberg O. W., Mohapatra R. N. // Phys. Rev. Lett. 1987. V. 59. P. 2507; 1989. V. 62. P. 712; Phys. Rev. D. 1989. V. 39. P. 2032.
141. Okun L. B. // JETP Lett. 1987. V. 46. P. 529.
142. Govorkov A. B. // Phys. Lett. A. 1989. V. 137. P. 7.
143. Suzuki Y. *et al.* // Phys. Lett. B. 1993. V. 311. P. 357.
144. Arnold R. *et al.* (NEMO Collab.) // Eur. Phys. J. A. 1999. V. 6. P. 361.
145. Ejiri H., Toki H. // Phys. Lett. B. 1993. V. 306. P. 218.
146. Bernabei R. *et al.* // Phys. Lett. B. 1997. V. 408. P. 439.
147. Kishimoto T. *et al.* // J. Phys. G. 1992. V. 18. P. 443.
148. Kekez D., Ljubičić A. A., Logan B. A. // Nature. 1990. V. 348. P. 224.
149. Miljanić D. *et al.* // Phys. Lett. B. 1990. V. 252. P. 487.
150. Back H. O. *et al.* (Borexino Collab.) // Eur. Phys. J. 2004 (submitted).
151. Belostotski S. L. *et al.* // Sov. J. Nucl. Phys. 1985. V. 41. P. 903.

152. Audi G., Wapstra A. H. // Nucl. Phys. A. 1995. V. 595. P. 409.
153. Kamyshkov Y., Kolbe E. // Phys. Rev. D. 2002. V. 66. P. 010001.
154. Back H. O. et al. (Borexino Collab.) // Phys. Lett. B. 2003. V. 563. P. 23.
155. Aglietta M. et al. // Nuovo Cim. C. 1986. V. 9. P. 185.
156. Lee J. H., Lee C. S. // Nucl. Instr. Meth. A. 1998. V. 402. P. 147.
157. Khalchukov F. F. et al. // Nuovo Cim. 1995. V. 18. P. 517.
158. Langacker P. // Phys. Rep. 1981. V. 71. P. 185.
159. Carlson C. E., Carone C. D. // Phys. Lett. B. 2001. V. 512. P. 121.
160. Babu K. S., Pati J. C., Wilchek F. // Nucl. Phys. B. 2000. V. 566. P. 33.
161. Babu K. S., Mohapatra R. N. // Phys. Lett. B. 2001. V. 518. P. 269.
162. Pati J. S., Salam A. // Phys. Rev. Lett. 1973. V. 31. P. 661.
163. Feinberg G., Goldhaber M., Steigman G. // Phys. Rev. D. 1978. V. 18. P. 1602.
164. Mohapatra R. N. et al. // Phys. Lett. B. 2000. V. 491. P. 143.
165. Rubakov V. A. // Phys. Usp. 2001. V. 44. P. 871.
166. Dubovsky S. L. // JHEP. 2002. 01. 012.
167. Flerov G. N. et al. // Sov. Phys. Dokl. 1958. V. 3. P. 79.
168. SNO Collab. // Nucl. Instr. Meth. A. 2000. V. 449. P. 172.
169. Tretyak V. I., Zdesenko Yu. G. // Phys. Lett. B. 2001. V. 505. P. 59.
170. Zdesenko Yu. G., Tretyak V. I. // Phys. Lett. B. 2003. V. 553. P. 135.
171. Evans J. C., Jr., Steinberg R. I. // Science. 1977. V. 197. P. 989.
172. Fireman E. L. // Proc. of Intern. Conf. «Neutrino'77», Baksan Valley, 1978. V. 1. P. 53.
173. Steinberg R. I., Evans J. C. // Ibid. V. 2. P. 321.
174. Tretyak V. I., Denisov V. Yu., Zdesenko Yu. G. nucl-ex/0401022.
175. Suzuki Y. et al. // Phys. Lett. B. 1993. V. 311. P. 357.
176. Ahmed S. N. et al. (SNO Collab.). hep-ex/0310030.
177. Learned J., Reines F., Soni A. // Phys. Rev. Lett. 1979. V. 43. P. 907.
178. Berger C. et al. // Phys. Lett. B. 1991. V. 269. P. 227.
179. Glicenstein J. F. // Phys. Lett. B. 1997. V. 411. P. 326.
180. Bernabei R. et al. // Phys. Lett. B. 2000. V. 493. P. 12.
181. Lederer C. M., Shirley V. S. Table of Isotopes. 7th ed. N. Y.: Wiley, 1978.
182. Boem F., Vogel P. Physics of Massive Neutrinos. Cambridge University Press, 1987.
183. de Holanda P. C., Smirnov A. Yu. hep-ph/0211264.
184. Vogel P. // Phys. Rev. D. 1984. V. 30. P. 1505.
185. Oberauer L., Von Feilitzsch F., Mossbauer R. L. // Phys. Lett. B. 1987. V. 198. P. 113.
186. Kopeikin V. I., Mikaelyan L. A., Fayans S. A. // JETP Lett. 1990. V. 51. P. 86.
187. Hagner C. et al. // Phys. Rev. 1995. V. 52. P. 1343.
188. Toussaint D., Wilczek F. // Nature. 1981. V. 289. P. 777.
189. Oberauer L. et al. // Astropart. Phys. 1993. V. 1. P. 377.

190. *Dolgov A. D. et al. // Nucl. Phys. B. 2000. V. 580. P. 331.*
191. *Dolgov A. D. // Phys. Rep. 2002. V. 370. P. 333.*
192. *Raffelt G. G. hep-ph/0208024.*
193. *Back H. O. et al. (Borexino Collab.) // JETP Lett. 2003. V. 78. P. 261.*
194. *Shrock R. E. // Phys. Rev. D. 1981. V. 24. P. 1275.*
195. *Bryman D. A. et al. // Phys. Rev. Lett. 1983. V. 50. P. 1546.*